

**The Three Dimensional Structure of EUV Accretion Regions in AM Herculis
Stars:
Modeling of EUV Photometric and Spectroscopic Observations**

Martin. M. Sirk¹

Center for EUV Astrophysics, University of California, Berkeley, CA 94720

Steve. B. Howell²

Department of Physics and Astronomy, University of Wyoming, University Station, Laramie WY
82071

ABSTRACT

We have developed a model of the high-energy accretion region for magnetic cataclysmic variables and applied it to *Extreme Ultraviolet Explorer* observations of 10 AM Herculis type systems. The major features of the EUV light curves are well described by the model. The light curves exhibit a large variety of features such as eclipses of the accretion region by the secondary star and the accretion stream, and dips caused by material very close to the accretion region. While all the observed features of the light curves are highly dependent on viewing geometry, none of the light curves are consistent with a flat, circular accretion spot whose lightcurve would vary solely from projection effects. The accretion region immediately above the WD surface is a source of EUV radiation caused by either a vertical extent to the accretion spot, or Compton scattering off electrons in the accretion column, or, very likely, both. Our model yields spot sizes averaging $0.06 R_{WD}$, or $f \sim 1 \times 10^{-3}$ the WD surface area, and average spot heights of $0.023 R_{WD}$. Spectra extracted during broad dip phases are softer than spectra during the out-of-dip phases. This spectral ratio measurement leads to the conclusion that Compton scattering, some absorption by a warm absorber, geometric effects, an asymmetric temperature structure in the accretion region and an asymmetric density structure of the accretion column are all important components needed to fully explain the data. Spectra extracted at phases where the accretion spot is hidden behind the limb of the WD, but with the accretion column immediately above the spot still visible, show no evidence of emission features characteristic of a hot plasma.

Subject headings: accretion, cataclysmic variables, AM Herculis stars — stars: individual (UZ Fornacis, VV Puppis, AM Herculis, HU Aquarii, RE1149+28, RE1844–74, EF Eridani, AN Ursae Majoris, V834 Centauri, QS Telescopii — EUV

¹Also with Department of Physics and Astronomy, San Francisco State University, San Francisco, CA 94132

²Guest observer, *EUVE* satellite

1. Introduction

AM Her stars are a class of interacting binaries consisting of a highly magnetic (typically 10 – 60 MG) white dwarf (WD) primary and a red main sequence secondary that fills its Roche Lobe. Stellar material flows through the inner Lagrangian point (L1) and falls toward the primary forming an accretion stream. In the absence of a magnetic field, an accretion disk normally forms. However, in AM Her systems, the strong magnetic field captures the ionized material and channels it directly toward one or both of the magnetic poles of the WD primary, forming a hot accretion region. The interaction of the accretion stream with the magnetic field circularizes the orbits of both stars and synchronizes the WD rotation period with the binary orbital period. When viewed from the rotating frame, the primary, secondary, and magnetic field all appear static. The only motion is that of the in-falling material, its free-fall time being about one fourth the orbital period.

Conversion of the kinetic energy of the stream manifests itself in many forms. Electrons in the stream near the accretion region spiral around the field lines and emit highly polarized cyclotron radiation at optical and near infrared wavelengths. X-rays arise in a shock region where the supersonic stream gives up energy, becomes heated and flows subsonically onto the WD surface. Extreme ultraviolet (EUV) radiation is emitted from, or very close to, the heated WD surface; the consequence of reprocessed X-rays and the direct mechanical heating of the WD photosphere by the impacting material. See Liebert & Stockman (1985), Cropper (1990), and Warner (1995) for reviews on AM Her systems.

The field strengths of the white dwarfs in magnetic CVs are strong enough to focus accreted material onto their surface in a relatively small area ($f \sim 1 \times 10^{-3}$ of the WD surface) called the accretion region. Observational evidence for this situation comes from many sources, all of which provide convincing proof for the white dwarf spin to be locked with the binary orbit and for the compactness of the accretion region. The accretion onto a magnetized white dwarf is nearly a radial in-fall situation, making the problem almost one-dimensional in nature. Radial accretion onto a WD surface was first considered to explain X-ray emission in Sco X-1 (Cameron & Mock, 1967).

The general idea of magnetically focused accretion is as follows. Ionized material leaving the L1 point of the secondary is in free fall until at some point, called the coupling region, the kinetic energy associated with the angular momentum is overcome by the magnetic energy of the primary field, and the material gets funneled along the field lines to the WD surface. The flow can initially be assumed to be uniform from the secondary all the way to the primary star. We will see that this is likely *not* to be the case but will serve as a working model for now. A strong shock is encountered by the accreting stream just above the surface where it decelerates by a factor of 3-4, converting much of its infall energy to short wavelength radiation. Post-shock material moves at subsonic velocities and settles onto the WD surface. Temperatures in the post-shock region are near $kT_{TB} \sim 10\text{-}25$ keV and $kT_{BB} \sim 20\text{-}40$ eV, with emission peaking in the X-ray and EUV regions. This short wavelength radiation leaves the accretion column easily, with about

half escaping into space and half going towards the WD photosphere around the accretion region. The accretion area near the WD surface becomes heated to a few times 10^5 K, giving rise to EUV emission.

The accretion region was originally modeled as a circular region (often referred to as an accretion spot) lying flat on the WD surface (Lamb and Masters, 1979). These authors also calculated the overall emitted spectrum as a sum of cyclotron emission, bremsstrahlung, and reprocessed black-body emission from the heated surface. Observations of AM Hers at high energies (X-rays), revealed a fascinating array of complexities in the accretion regions. By the late 1980’s, new ideas for the size and shape of the accretion regions were emerging. Foremost among these was the work of Wickramasinghe and Meggitt (1985), Wickramasinghe, Ferrario & Bailey (1989), and Ferrario, Wickramasinghe & Tuohy, (1989). Their view gave the accretion spot an arc-like shape of length $\sim \frac{1}{4} R_{WD}$, instead of a circular profile, regions of high and low density mass flow, and the spot had a small height ($\sim \frac{1}{10} R_{WD}$) above the surface. Surrounding the entire spot was an extended corona-like halo of hot plasma .

The early models of a homogeneous flow with cylindrical symmetry in the accretion stream made the prediction that the emitted luminosities at high energy will be such that the hard X-ray emission will be greater than about 2 times the soft X-ray (EUV) emission. Observations in the EUV spectral region, particularly in recent years by the Röntgen Satellite (*ROSAT*) and the Extreme Ultraviolet Explorer (*EUVE*), have again caused accretion region models to be re-evaluated (eg. Ramsay et. al. 1994, Beuermann & Schwöpe 1994). These authors and others, have shown that soft X-ray excesses exist in most of the AM Herculis systems, unexplainable in the older models.

Discussions of the “soft X-ray problem” are given in Cropper (1990), King (1995), and Beuermann & Burwitz (1995) and references cited therein. New ideas including inhomogeneous flows, blobby accretion, buried accretion regions, and cyclotron cooling of the post–shock region have been pursued in an attempt to understand the observations. Blobby accretion was first discussed in Kuijpers & Pringle (1982) and followed up on by others. Litchfield (1990), allowed the blobs to bury themselves deep into the WD atmosphere before giving up their store of energy, causing increased local heating and giving rise to an “excess” of EUV photons. Litchfield also calculated a shape and size for the accretion region, and the lightcurve expected for 100 Å observations (see §7.2).

King (1995) has suggested that one can match the observations via an accretion region consisting of various sites of bombardment within the total effective radiating area, the latter being the area in which the blobs usually land. Each of the sites may become a depressed accretion region, buried beneath the WD surface by several atmospheric scale heights.

All of the models discussed above generally agree that the accretion region is relatively small and its “size” is wavelength dependent. The hard X-rays come from the central concentration, presumably located near the stream shock. Surrounding this central concentration, there is an

extended region of EUV emission (~ 1000 km in extent), heated from above by X-rays from the shock and from below by thermal energy released by the impacting blobs. (see Cropper;1990, Stockman et. al.; 1994, & Schwobe; 1995).

Disentangling the various radiations from their points of origin is difficult, especially in the optical where the photospheres of both stars as well as the accretion stream all contribute flux. Observations in the EUV (65Å to 180Å) are particularly well suited to probing the accretion region since the source of radiation is often confined to a very small region on, or near, the WD surface. Furthermore, many AM Her systems are intrinsically bright around 100 Å. The peak energy release of the extended spot, and the pre- and post-shock regions of the stream are all sources of EUV emission.

The *EUVE* satellite has performed a number of pointed photometric and spectroscopic observations of AM Herculis stars (cf., Craig et. al., 1997), and in this paper we present results for many of these stars. Using the high quality, high time-resolution EUV data, we have developed a new model for the accretion geometries of AM Her systems. This model, discussed in §4, provides quantitative information on the size, shape, and variability of the accretion region. In addition, our model provides the first direct evidence of extended EUV emission above the WD surface, originating in either an extended halo, or the lower (pre-shock) portion of the stream itself.

2. Geometric Variability of Accretion Regions

Multi-wavelength light curves of AM Her stars show strong modulation arising from both geometrical and physical effects. The intrinsic amount of radiation from AM Her stars varies on time scales ranging from seconds to years and is mainly controlled by the mass transfer rate. During one binary orbit, the viewing geometry to the accretion region changes considerably. The angle subtended between the observer and the accretion spot normal vector varies as a function of the system inclination ι , the spot colatitude β (measured from 0° to 180° from the rotational pole tilted towards the observer), and the rotation phase ϕ_b of the synchronously locked binary (see Fig. 1). For a small ($r \ll R_{WD}$) flat accretion region confined to the WD surface, the observed modulation is purely sinusoidal as a function of phase and reaches maximum brightness when the viewing angle is at a minimum (that is, when the spot normal is pointed most directly towards the observer). This occurs when the accretion spot crosses the central meridian of the WD and presents its largest cross section. In systems where $(\iota + \beta) > 90^\circ$ a flat accretion spot rotates behind the limb of the WD surface and is completely occluded for some portion of the binary orbit. In Figure 2 we show synthetic light curves for a small accretion region illustrating the sinusoidal modulation caused by changes in viewing geometry for different system inclinations and accretion spot colatitudes. We discuss, in more detail, the model light curves of Figure 2 in §4.1.

Highly inclined systems ($\iota \approx > 73^\circ$) also show eclipses of the WD primary by the secondary dwarf star. If the accretion region appears in the upper hemisphere ($\beta < 90^\circ$) of the WD, then

the accretion stream, when it is still far from the WD surface (the far-field stream) *must* cross the line of sight to the accretion region at some point during the orbit and may result in a dip in the lightcurve (Mason, 1985, King and Williams, 1985). These far-field dips often saturate to zero flux mimicking a stellar eclipse. Finally, the accretion stream in the immediate vicinity of the accretion region (referred to as the pre-shock or near-field accretion column) may also absorb or scatter EUV radiation out of the line of sight producing dips in the lightcurve (Imamura & Durisen, 1983, hereafter ID83). These near-field accretion dips tend to be broad in phase and generally do not saturate to zero flux. The amount of attenuation is strongly dependent on the viewing geometry through the column to the spot, being greatest when one looks parallel to the column, and least when viewing perpendicular to the column.

We present in Figure 3, the 1995 January *EUVE* lightcurve for the eclipsing system UZ Fornacis to exemplify the features discussed in this paper. Clearly, the light curve of UZ For is more complicated than the simple sinusoidal variations predicted by a basic model in Figure 2. Identifying the causes of the observed modulations and features in the EUV light curves by developing a general model of the accretion region applicable to any AM Her star is the goal of our analysis presented here.

Analysis of *Extreme Ultraviolet Explorer* (*EUVE*; Bowyer & Malina 1991) photometry of UZ For (Warren, Sirk, & Vallergera 1995, hereafter WSV) showed a small ($< 0.23 R_{WD}$) EUV accretion spot that is raised a few percent above the WD surface. Furthermore, the symmetric eclipse profiles of the spot precluded any large scale longitudinal structure (such as an auroral arc with a brightness gradient). Vennes et. al., (1995) also determined a height of a few percent of the R_{WD} for the accretion spot of VV Pup based on model atmosphere calculations. Vertical extension of the accretion region profoundly affects the EUV light curves (cf., Sirk & Howell 1996), both by lengthening the duration of the bright phase (when the spot is not behind the WD limb), and steepening the rise and fall phases (when the spot rotates into and out of view from behind the WD limb). To understand the physical processes of AM Her systems one requires an accurate knowledge of the system geometry, namely the orbital inclination (ι) and the colatitude of the accretion spot (β). Determination of these parameters is often done via optical light curve and polarimetry observations. The assumption of a flat accretion spot when analyzing these types of data may result in incorrect values of ι and β . Our initial analysis modeled the EUV accretion regions, allowing the inclination, spot colatitude, spot size, and spot height to all be free parameters.

3. Data and Light Curves

The observational data for the ten systems analyzed here consists of our own *EUVE* guest observer data (Howell et. al., 1995, Sirk et. al., 1998), data from the *EUVE* public archive, and data from the *EUVE* Right Angle Program (McDonald et. al., 1994). All of the photometric data used was obtained in the Lexan/Boron passbands of the deep survey and scanner telescopes

($\geq 10\%$ of peak transmission from 67 to 178 Å, peak at 91 Å; Sirk et. al., 1997) and the short wavelength spectrometer ($\geq 10\%$ of peak transmission from 65 to 178 Å, peak at 100 Å; Boyd et. al., 1994). The deep survey and three spectrometer channels of *EUVE* are co-aligned; photometry and spectroscopy for a given target are obtained simultaneously. An observation log of the ten systems studied is presented in Table 1. The source photons are counted in a circle usually of 1 arcmin in radius, and the background estimated in a concentric annulus with typical inner and outer radii of 3 and 11 arcmin. To preserve the high temporal resolution of *EUVE*, the arrival time of each photon is first folded by the appropriate binary period, then a histogram is constructed at some chosen phase bin interval (ranging from 3 s for the bright sources to 12 s for the faintest source). Heliocentric corrections are applied to every photon arrival time before folding onto the binary periods. Finally, the exposure time (corrected for detector deadtime) is calculated for each phase interval (see Hurwitz et. al., 1997 for details).

The EUV light curves of the AM Herculis stars fall into two distinct categories: the first is where the accretion region rotates behind the limb of the WD for some portion of the phase (UZ For, HU Aqr, VV Pup, RE1844-74, RE1149+28, and AM Her, $\beta + \iota > 90^\circ$), and the second is where the accretion region remains visible at all phases (EF Eri, AN UMa, and V834 Cen, $\beta + \iota < 90^\circ$). Qualitatively, the first category of light curves resemble the positive portion of a cosine curve, and generally show one or two dip features. The second category (which should resemble an entire cosine cycle) are dominated by three or four dip features each. We present our sample of EUV light curves for six self eclipsing AM Her stars in the first eight panels of Figure 4. The non-self eclipsing systems are shown in the remaining four panels of Figure 4. The plotted symbols (open and filled circles) represent the observed countrate at a given binary orbital phase and the solid and dashed lines represent model fits: both are discussed in §4.

One object, QS Tel (Rosen et. al., 1996), shows evidence for accretion onto only one pole during one epoch, and onto both magnetic poles at other times (Fig.4). Since its inclination is not yet known, we can not classify it uniquely into either EUV light curve family nor fit it with our model. Two of the systems are high inclination (UZ For & HU Aqr) and have the WD and accretion region totally eclipsed by the secondary star. Eclipse timings at all wavelengths provide stringent limits on the system inclination, and constrains the horizontal size of the accretion region. Analysis of the self eclipse of the accretion region by the WD limb in the first category of light curves provides a direct measure of the spot height and its vertical brightness profile, as well as constraints on the system inclination and spot colatitude. In the second category of light curves these same parameters are difficult to determine as they are poorly constrained. Thus, we have concentrated our initial modeling efforts on the first category of systems.

Since the total on-source integration times were significantly longer than the binary orbital periods (by factors of 5 to 35), all phases are sampled multiple times (although not necessarily equally). Therefore, the phase folded light curves represent time averages, not instantaneous states. The scatter in the countrates for a single binary orbit are much larger than that of the mean light curves shown in Figure 4 (eg., see Howell et al., 1995). Analysis of the short time scale

variations will be the subject of a future paper.

4. Light Curve Modeling

4.1. Geometric Accretion Spot Models

All of the AM Her stars presented in Figure 4 that undergo self eclipse, when the accretion spot rotates behind the limb of the WD, show a symmetric EUV rise and fall phase when reflected about the EUV mid-phase point. The symmetry is so remarkable, in fact, that we can define the phase midway between the rise and fall phase of the light curves, when the accretion region lies on the central meridian of the WD pointing most directly towards the observer, as phase 0 throughout this analysis. Enlargements of the light curves of the rapid rise and fall phases are presented in Figure 5 with the fall phase mirror reflected about the EUV mid-phase. In all six systems, the early rise phase and the late fall phase show almost a perfect match, which indicates that the accretion regions cannot possess any large scale horizontal asymmetries.

The two eclipsing systems (UZ For, WSV; and HU Aqr, Sirk et. al., 1998, Schwobe et. al., 1998) show very rapid ingress and egress eclipse times in the EUV of ~ 2 s each. This short time scale constrains the size of the accretion regions to 16% and 23% of the R_{WD} , respectively, and restricts the region of EUV emission to within $\approx 0.15 R_{WD}$ of the WD surface. This strong evidence for a small, symmetric, vertically extended accretion spot in the two eclipsing systems, and their similarity to other non-eclipsing AM Her systems, motivated us to model the EUV accretion regions in all ten AM Her stars with simple geometrical models.

Three symmetric, uniformly bright accretion spot models were constructed; A flat circular spot, a cone with circular base, and a raised mound (sector of rotation). In each model, the brightness is directly proportional to the cross-sectional area visible at a given phase (ie., in this first stage, we assume the column is optically thin and the spot exhibits no limb darkening. We explore the effects of an optically thick column in §4.3). The synthetic light curves from a small, flat spot closely resemble the positive portion of a cosine curve, and thus, completely fail to account for the steep rise and fall phases of the EUV light curves (as well as any dips). The conical spot model also failed to reproduce the steepest portions of the light curves. A raised mound, however, fit the rise and fall phases very nicely. When seen face on, the mound model is indistinguishable from a flat spot. However, when viewed edge on, a flat spot disappears, whereas a mound still shows appreciable area and continues to do so as the footprint of the spot rotates behind the WD limb. We explored a full range of spot sizes, spot heights and colatitudes and present a typical example in Figure 2 showing synthetic light curves for a flat circular spot and a raised mound at four different binary inclinations $\iota = (80, 60, 40 \text{ and } 20^\circ)$ and a range of spot colatitudes spanning both hemispheres. In this example the spot radius is $0.06 R_{WD}$, and for the mound model the height is $0.03 R_{WD}$. We also created asymmetric spots by placing two spots of identical radius, but one twice as bright as the other, side-by-side along the direction of rotation.

Noticeable departures from symmetry in the synthetic light curves occurred when the long axis of the composite spot model exceeded $0.2 R_{WD}$. This type of large scale asymmetric accretion region seems to be completely ruled out by the observations.

4.2. Application of the Geometric Accretion Spot Model

The geometric spot model for a symmetric accretion region (flat or raised) produces symmetric light curves. The six systems shown in Figure 4 that undergo self eclipse where the accretion spot rotates behind the limb of the WD, show a symmetric EUV rise and fall phase when reflected about the EUV mid point. This fact alone indicates that, regardless of whether the accretion spots are flat or show vertical extent, they all must be small ($r_{spot} < 0.2 R_{WD}$) in longitudinal extent, or have a uniform brightness profile in the longitudinal direction, since the observed symmetry would not be produced by a large accretion region extended in magnetic longitude with a non-uniform brightness profile. The steep, nearly linear rise and fall phases seen in the self eclipsing systems (Figs. 3–5) are inconsistent with the gently curving cosine behavior expected from projection effects of a flat spot (Fig. 2) and indicate a vertical extent of the EUV emission above the accretion region.

We applied our geometric model first to UZ For since its inclination and spot colatitude were accurately determined from optical eclipse photometry by Bailey & Cropper (1991), and the EUV spot size is known from eclipse ingress and egress timings (WSV). To test the utility of the model, we allowed the inclination and the spot colatitude to be free parameters, even though they were already known. The central parts of each light curve are subject to eclipses by the secondary star, the far-field accretion stream, and show other dip features probably caused by material very close to the accretion spot itself. We initially excluded these regions from the model fits since it is impossible to reproduce them from projection effects alone (we explicitly address these features in §4.3). We fit the filled circles (Fig. 4) using our raised mound model and an iterative, non-linear least squares fitting routine. The algorithm requires initial starting values for each parameter. To ensure convergence at the global minimum, and not a local minimum of the parameter space, the fit is iterated repeatedly with different starting values. Fitting our raised mound model to UZ For, we find a spot radius and spot height of .06 and .03 R_{WD} , respectively, and an inclination and colatitude of 80° and 136° . These latter two values are in excellent agreement with those determined by Bailey & Cropper (1991). The same model was then applied to HU Aqr, VV Pup, AM Her, RE1149+28 and RE1844–74. Our fits are shown as dashed lines in Figure 4. For the two eclipsing systems, UZ For and HU Aqr, where the absolute phase zero is known (defined as the center of the eclipse of the WD by the secondary), the accretion spot longitude (ψ) is obtained directly as the difference in phase between the center of the eclipse and EUV mid-phase zero. Our derived system and accretion region parameters are listed in Table 2.

Errors in the fit parameters are dominated by the assumptions in the model (i.e., circular symmetry and uniform brightness) and subjective choices made in the construction of the light

curves, not by the Poisson error in the actual data themselves. Phase zero for each system is determined directly from the light curves by mirror reflecting the fall phase onto the rise phase until they overlap. This process is done visually and is thus somewhat subjective. The choice of binary phase bin size (mainly dependent on EUV countrate) also affects the fits slightly. The subjective error is estimated by varying the bin size and the phase zero point, and comparing the resultant fits. Stable solutions were found for all systems and typical errors for each parameter determined. The binary inclination has the greatest effect on the lightcurve models and is therefore strongly constrained to within 5° . The spot colatitudes are stable to within $7\text{--}15^\circ$, and the spot height and radius to within 25% and 35%, respectively.

In Table 3 we compare our system geometry results to those of others using different methods. The modeling of optical and near IR polarization data has become quite sophisticated, providing not just system inclination and accretion spot colatitude, but also the size and shape of the accretion region (cf. Wickramasinghe et. al., 1991, Ramsay et. al. 1996, Potter et. al., 1998). Analysis of spectrophotometric data by the means of Doppler tomography yields the location of origin of optical line emission, confining it unequivocally to (a) the secondary star, (b) the ballistic portion of the accretion stream, or (c) the magnetically funneled part of the stream (Schwope et. al., 1997). The deconvolution of the various line velocities imposes limits on the system inclination and mass ratio. While the agreement between the values of system parameters seen in Table 3 is excellent, it must be emphasised that the location of the source of radiation employed in each method is quite different. The EUV radiation is confined to a small region very near the WD surface, whereas the source of optical radiation very likely extends much higher up the stream and contains contributions from other system components. Thus, any model that aims to accurately predict the system inclination, and the size, shape, and location of the accretion region must incorporate a three dimensional source of radiation. Assuming that the optical radiation emanates from the flat footprint at the base of the accretion column (as is commonly done in polarimetry modeling) introduces systematic errors in the determination of the system inclination and spot colatitude (M. Cropper, 1998, private communication). Wu & Wickramasinghe (1992) have made progress in modeling the optical emission region as a three dimensional structure. Modeling the EUV accretion region as a raised spot of emission provides an independent means of estimating the system geometry.

For the six systems where the accretion spot undergoes self eclipse, the symmetric, raised spot model accounts for the early and late EUV phase (ie. where the accretion spot is seen mainly edge-on near the WD limb) very well. The geometric raised mound model showed us that the vertical extent of the accretion region is the primary cause of the symmetry in the early and late portions of the EUV light curves. Longitudinal brightness gradients, as we have seen, have virtually no effect on the light curves at any phase for raised accretion regions whose longitudinal extent is less than $0.2 R_{WD}$. Hence, any system that shows symmetric rise and fall phases must either have a small accretion region, or a uniform brightness profile in longitude.

A careful study of the residuals of all the fits to the category 1 systems showed a systematic

and symmetric underestimate of the flux at the very earliest rise phase, and very latest fall phase (cf., Figs. 3 and 4). The region of residual flux typically spans 10% of the phase for each star. Rather than invoke a horizontal brightness profile of the accretion region that symmetrically leads and follows the spot center by 5% in phase on each side, we attribute the residual flux ($\sim 1\%$ of the total flux) to EUV radiation emanating from the accretion region (column) immediately above the accretion spot proper. Our data are consistent with the brightness of the column decreasing exponentially with distance from the WD surface. Thus, we need add only two additional parameters (a brightness scale factor, and an exponential decay constant) to our raised mound model to adequately reproduce the residual portion of the light curves. The maximum height of this extended EUV luminous accretion column may be measured directly from the light curves once ι and β are known. Figure 6 compares the fits of a flat circular spot, a circular raised mound, and a circular raised mound with luminous accretion column to the fall phase of UZ For. The flat spot fit shows large residuals and places the accretion spot 130° away (in the opposite hemisphere) from its known location. The raised-mound fit does well in the steep fall phase but systematically underestimates the late fall phase. The final panel models the accretion column as a source of EUV flux that decreases exponentially with height above the WD surface. All points in the rise and fall phases are fit by this model.

In Figure 7 we plot our derived accretion column intensity as a function of distance above the WD surface for three systems, normalized to the peak intensity measured for each system. The source of this vertically extended EUV emission is not well understood, but later in this paper, we discuss the likely possibility that the excess EUV flux at these phases is from Compton scattering by electrons in the near-field accretion column. Emission (lines) from a corona-like halo surrounding the accretion region ³ are predicted by theory, but as we will see, are unobserved in AM Hers.

4.3. Near- and Far-Field Accretion Column Effects

A quick look at Figure 4 shows that the EUV light curves in general are anything but symmetric. As the accretion spot rotates towards the central meridian and is viewed mainly face-on, the light curves show a variety of dips which cannot be accounted for by any simple geometric model. Every system shows at least one dip, and some two or more. For systems where $(\beta - \iota) < 0^\circ$ the far-field accretion stream is guaranteed to cross the line of sight to the accretion spot possibly causing a dip. For highly inclined systems ($\iota \approx > 73^\circ$) the stream may still intersect the line of sight even if $(\beta - \iota) > 0^\circ$ due to the finite width of the stream (WSV). This is indeed the case for UZ For and VV Pup; both systems show deep stream dips (labeled as such in Fig. 4), high binary inclination, and accretion spots in the lower hemisphere ($\beta > 90^\circ$). Because the

³Evidence for such coronal emission is seen in the DQ Herculis star EX Hya (Hurwitz et. al., 1997) and possibly in PQ Gem (Howell et. al., 1997)

in-falling material retains the angular momentum of the secondary star, the accretion stream must lead the line connecting the star centers in the direction of binary rotation. Thus, any observed eclipses of the accretion spot by the far-field stream must occur before absolute phase zero. Since the accretion spot in AM Her stars generally leads absolute phase zero by roughly 45° (Cropper, 1990), the far-field accretion stream dip will occur near the middle of the EUV bright phase (phase zero throughout this analysis). The observed stream dips are narrow in phase and imply that the absorbing material is far from the WD surface.

In addition, broader dips are seen in every system, occurring for the most part at earlier phases than the far-field stream dips (labeled “Dip”, and “Stream Dip”, respectively, in Fig. 4). A firm conclusion from our model is that *none* of the observed dips can be reproduced merely from differences in viewing geometry. As the accretion spot emerges from the WD limb, its projected area (and hence its brightness) can only *increase* until it crosses the central WD meridian, regardless of the spot’s shape or horizontal brightness profile (see Fig. 2). The observed width of the broad dips suggests that light is being removed from the line of sight by material close to the point of origin. Thus, we hypothesize that absorption or scattering by the near-field accretion column itself, in the immediate vicinity of the accretion spot, is the cause of these features. As the WD rotates, the path length (both geometric and optical) along the line of sight through the near-field column to the accretion spot varies continuously and considerably.

To account for the broad dip, we construct an absorption model that assumes a cylindrical accretion column of uniform density incident upon the WD surface at some angle with respect to the spot normal, and with a radius equal to the spot radius. Two angles are required to uniquely specify the direction angle of incidence of the column relative to the spot normal. The first is the angle of incidence of the column tilted in the direction of latitude. The second angle is the angle of incidence of the column tilted in the direction of rotation (longitude) and is estimated directly from the light curves as the difference in phase between the center of the broad dip and the EUV mid-phase (phase zero). This latter angle is input to the model as a fixed parameter. Figure 8 illustrates the geometry of this model which requires just two free parameters; the angle of incidence of the column tilted in the direction of latitude, α , and an absorption coefficient τ where the transmission through the column obeys

$$T = e^{-\tau l} .$$

The effective transmission is calculated by integrating over all possible path lengths l through the cylindrical column to the spot for a given viewing direction. The path length l is determined analytically from the rotation phase ϕ_b , the inclination ι , the spot colatitude β , and the angles of incidence of the column in latitude α and longitude, and the column (spot) radius r . By varying the parameters τ and α , symmetric dips of nearly any width and depth are possible. Since the values of inclination, spot colatitude, and spot height have already been determined by the geometrical model, we hold them constant as fixed parameters.

Using this straightforward absorption idea, in connection with our previous spot model, five

systems (excluding HU Aqr since it showed no obvious broad dip in the May 1996 observation⁴) were modeled well. We again exclude from our fits data points at phases where the narrow dip by the accretion stream far from the WD (and the stellar eclipse seen in UZ For) dominate. The ratio of the total absorber model flux to the total un-absorbed model flux (ie. the ratio of the areas under the solid and dotted line fits in Figure 4), integrated over the phase interval where the accretion region is not hidden behind the white dwarf, and the derived values of the absorption coefficient τ are presented in the final two columns of Table 2. The optical depths determined by modeling the broad dips range from 0.1 to 2. The tilt angles (α) of the accretion column with respect to the spot normal ranged from 4° to 51° . They are not listed in Table 2 since we do not believe that accretion columns generally tilt more than $\sim 10^\circ$ (eg., Meggitt & Wickramasinghe, 1989). However, our model clearly requires large tilt values (in both the longitudinal and latitudinal directions) and we discuss the significance of these tilts in §7.2.

Our cylindrically symmetric column absorber model accounts for the gross features of the broad dips quite well as shown by the solid lines in Figure 4. We point out, however, that where the light curves in Figure 4 show sharp transitions (e.g. the right angle kinks visible at the end of the rise phase in both UZ For and VV Pup), the residuals from our absorber model fits indicate that the true situation must be more complex than can be accounted for from a cylindrically symmetric, uniformly dense accretion column. This is no surprise as the accretion columns are likely to be clumpy, asymmetric, and have structure to them (cf., Cropper 1990, Wu & Wickramasinghe, 1992). By themselves, the EUV light curves cannot constrain in detail a more sophisticated model with additional structure but we discuss likely possibilities in §7 and are currently developing a more realistic near-field stream model.

For the second category of light curves (where the spot is visible at all phases), an attempt was made to interpret the light curves of V834 Cen, AN UMa, QS Tel, and EF Eri in terms of our absorber plus spot model in spite of the fact that the inclination, spot colatitude, spot size and height are not directly determinable from the light curves. We performed a grid search in parameter space, the mean starting values for the inclination and colatitude for each system are taken from Cropper (1990), and the mean spot radius and height used were an average value found from the first category of systems. Stable solutions were found for each star, but deciding where the EUV mid-phase lies, and distinguishing between the far-field stream dips and the near-field accretion column broad dips, among the many visible dip features is highly subjective. Our absorber model (uniform density, symmetric spot and column) will only account for a single dip, whereas these systems show what appear to be multiple structures. We conclude that the numerous features in these light curves are indicative of additional structure in the accretion stream, column, and/or in the accretion region such as multiple column filaments and multiple EUV emission sites (cf., Harrop-Allin et. al., 1998).

⁴ However, recent EUV observations of HU Aqr, obtained in May 1997, showed a pronounced dip quite similar to that seen in UZ For and will be addressed in Sirk et. al., 1998

5. Phase-Resolved EUV Spectra

Can the EUV spectra tell us anything about the nature of the observed photometric behavior seen in the AM Her systems? Using the light curves as a guide, we extracted phase resolved spectra for the three bright systems (UZ For, VV Pup, & AM Her) in the manner described in Hurwitz et. al., (1997). We selected four distinct phase regions: the earliest rise and fall phases where the spot is still fully obscured behind the WD limb with only the flux from the column above the spot visible, the broad dip region, a bright region at late phase where the light curves show no dips, and for UZ For and VV Pup a spectrum during the far-field stream dip phase. These phase regions are delineated in Figures 3 and 4.

The EUV spectra averaged over the bright phase for AM Her stars typically show an (interstellar) absorbed blackbody continuum without any emission lines and possibly weak absorption features (Paerels et. al., 1996, Vennes et. al., 1995). This is in striking contrast to the EUV spectrum of the intermediate polar star EX Hya which is dominated by iron emission lines characteristic of a plasma with temperature 10^7 K (Hurwitz et. al., 1997). The EUV spectra from the accretion region near the WD surface of AM Herculis stars are inconsistent with unperturbed emission from a hot, low density plasma.

However, what about the portion of the accretion column above the spot that is visible during the earliest rise and latest fall phases when the accretion spot footprint is hidden behind the WD limb? Hydrodynamic calculations of accretion onto a white dwarf by Woelk & Beuermann (1996) predict electron temperatures of a few times 10^7 to 10^8 K in the post-shock flow. One then might expect to see an emission line spectrum from a corona-like region above the accretion spot if it could be viewed separately. The spectra for UZ For, AM Her and VV Pup, extracted at phases when the spot is just barely obscured behind the limb of the WD but the EUV emission above the spot is still visible, are not statistically significantly different in morphology than the spectra observed when the spot is viewed face on. There is no compelling evidence for low density discrete plasma line emission. However, because the signal-to-noise ratio is low in the spectra from just before and after spot appearance (due to the fact that the region just above the spot is only visible for about 0.05 in phase), the existence of emission lines cannot be entirely precluded.⁵ The likely source of the EUV radiation from the column above the spot is Compton scattering off free electrons by the photons emanating from the accretion region below (cf., ID83 & below).

UZ For and VV Pup show clear evidence of flux removal at phases when the far-field accretion stream crosses the line of sight to the accretion spot. Comparing the bright phase spectra (labeled in Figs. 3 and 4) to the far-field stream dip spectra shows no dependence on wavelength during the flux reduction or any sign of absorption edges. The slope of the ratio of the far-field stream dip

⁵ The highly magnetic CV AR UMa, observed at high signal to noise by EUVE during a high state in December of 1996, shows no evidence of low density plasma emission lines at any phase, including those when viewing just above the accretion spot. Howell & Sirk, (1998).

spectra to the bright phase spectra is consistent with zero to within 3σ of the slope uncertainty. Therefore, we conclude that the stream dips are not primarily caused by absorption from neutral hydrogen (i.e., a cold absorber) but could have components due to photoelectric absorption by a warm (ionized) absorber (Cropper et al., 1997). It is unlikely that the far-field stream is completely or even mostly ionized (Harrop-Allin et al., 1997) thus, the number density of free electrons would be small. We would therefore not expect Compton scattering to play a large role here.

If the far-field stream near the coupling region was scattering the EUV photons (Compton scattering at EUV wavelengths causes only about an 8% change in the initial wavelength), then one might expect to see observational evidence for this. If we assume that the coupling region of UZ For were a source of EUV radiation it would be clearly seen immediately following ingress during the first half of the stellar eclipse when the accretion region is fully hidden, but with the entire accretion stream still visible. No EUV flux was detected during the stellar eclipse for the 1995 January UZ For observation (mean eclipse count rate = $0.0006 \pm 0.005 \text{ s}^{-1}$, see Fig. 3), however the 1993 November light curve shows a very low, but statistically significant detection of flux during eclipse (mean eclipse count rate = $0.005 \pm 0.002 \text{ s}^{-1}$ (WSV)). During these two observations, the shape and depth of the far-field absorption dip changed (see Figure 10). Thus, this may be observational evidence for the occurrence of far-field scattering of EUV photons. A more likely explanation, however, is that changes in the far-field stream position, density, and size cause variations in the optical depth and photoionization of the stream as a function of phase.

We now consider spectra obtained during the broad dip phases due to absorption by the column just above the accretion spot. Comparisons of the spectra extracted from the broad dip and the bright phases show significant wavelength dependence. We show spectra extracted during the broad dip phase and the bright phase for VV Pup, AM Her, and UZ For in the upper panels of Figure 9. The ratio of the dip phase to the bright phase is shown in the lower panels. Linear least-squares fits, weighted by the error in the ratio, show statistically significant positively sloped ratios for all three stars. The slopes are greater than zero by 12, 32, and 13 σ for VV Pup, AM Her, and UZ For, respectively. Over the entire wavelength range (75 to 125 Å) the broad dip phase spectra are *softer* than the bright phase spectra.

If the accretion column contained any significant neutral hydrogen or helium, then we would expect photoelectric absorption to occur, producing a typical power-law slope of -3 . The slope seen in Figure 9 is much shallower. Photoelectric absorption by heavier elements (such as C, N, O, Ne, Mg, Si, S, & Fe) is a likely cause of some of the photon loss in regions close to the shock where the stream is highly, but not necessarily fully ionized (Kylafis & Lamb, 1982). However, no convincing or substantial absorption lines have been seen in EUV spectra of AM Her (Craig et al., 1997), so the contribution to the observed opacity by ionized metals is small and, at best, limited to frequencies near absorption edges. The average photon energies present ($\sim 100 \text{ Å} = 200 \text{ eV}$) are greater than local blackbody kT values (near 20-40 eV), so Compton scattering is likely to be the dominant mechanism removing photons. This scattering process down-converts photon

energies and has a $1 - \cos\theta$ scattering dependence, so most photons (for 1 scatter) are scattered back down towards the WD surface or up towards the accretion column, but with lower energies in both cases. The resulting slope of the spectral distribution will have a direct relation to the optical depth of the gas if kT is not equal to, or even approximately near the average photon energy. The situation here has $kT \sim \langle E \rangle$. Since the energy of an EUV photon is much less than the rest energy of an electron, the Compton scattering cross section is independent of wavelength. Thus, flux removal from the line of sight by Compton scattering in the accretion stream would be approximately equal at all of our observed wavelengths, leading to a modest spectral slope. Thus, we would expect to see softer spectra (as we do within the broad dips) and some residual EUV emission at right angles to the column (also as observed, see end of §4.2). The nature of the near-field column is just beginning to be explored in relation to recent high-energy observations (Cropper et. al., 1997 and §7).

6. Longterm EUV Variability

The stars UZ For and RE1149+28 have each been observed three times by *EUVE*, twice during pointed observations with the deep survey/spectrometer, and once each serendipitously in the scanners by the RAP program. We display the light curves for all six observations in Figure 10. For each star, the two faintest light curves have been scaled to equal the mean countrate (Table 1) of the brightest observation. In addition to changes in mean EUV flux of up to factors of 3, the shapes of the light curves and positions in phase of the dip features have also changed. In the eclipsing system UZ For, the longitude ψ of the accretion spot shifted by over 6° in just one month, and the duration in phase of detectable EUV flux increased by 1% during the same interval. The depth and position in phase of both the narrow far-field accretion stream dip, and the broad near-field accretion column dip also changed. RE1149+28 shows similar, although less pronounced changes. These clearly varying features indicate dynamic movement of the gas stream, coupling region, and accretion regions on or near the WD surface itself. The eclipsing system HU Aqr has been observed six times over a 16 month period by *EUVE* specifically to study its longterm behavior and also has shown a few degree shift in the spot location. Further details of the longterm behavior of HU Aqr will be presented in Sirk et. al., (1998) & Schwobe et. al., (1998).

7. Discussion

7.1. Correlations between the Accretion Spot Model Parameters

Since we have determined some physical sizes and conditions for the EUV emitting regions in these AM Her stars, it might be useful to examine any possible correlations which may exist. We remind the reader that the collection of data used here is used in a mean fashion, thus any

short timescale (less than 1-2 binary orbits) or transient features of the accretion regions are averaged out. We present results for 10 different observational data sets on six different stars. The observations are almost all deep survey (DS) data but two were made with the scanner telescopes (ScA, ScB). Our noted correlations should be viewed with healthy skepticism due to the small sample of stars and intrinsic uncertainties in the physical and model parameters.

Using the information available in Tables 1 & 2 we find the following correlations. The ratio of the unabsorbed to absorbed flux, i.e., the “missing” flux due to the absorbing near-field column, and the height (h) of the EUV emitting mound are both related to the radius (r) of the accretion region itself: $Ratio = 4.57r + 0.45$ and $h = 0.23r + 0.0076$. This is not a surprise, as the larger the footprint of the region, the larger the near-field column and overall emitting height might be expected to be. The height of the emitting mound is also then correlated with the level of “missing” flux. We also find that the height of the emitting column determined from our model (h_{col}) is strongly related to the white dwarf magnetic field strength: $h_{col} = 0.0026B + 0.0094$. (This last relation does not include the star RE1844 in the fit. This seems reasonable as RE1844 is known to be a two-pole emitter most of the time; Bailey et al., 1995.) This $h_{col} - B$ relation is again, not surprising, as a stronger field should produce a more focused near-field column, leading to higher temperatures farther above the surface and thus higher EUV emitting regions. Comparisons of all other parameters with the magnetic field strength showed no obvious correlations.

The values of r and h have some indication of increasing their size with an observed increase in the mean EUV count rate. However, UZ For and RE1149+28 are the only multiple observations we have at hand and not all of these are with the same EUVE instrument. Thus, a definitive statement is not possible. We suspect that the overall mean count rate modulates with the mass accretion rate, but we have no simultaneous data in other wavebands with which to formulate a firm relationship between these parameters. Also, we note that from single binary orbital data in the EUV, small scale changes occur on tens of minute time scales, likely indicating regular short-term mass accretion variations. These aspects of short-term variability will be discussed by Sirk et al., (1998).

Using contemporaneous EUV and IR observations of HU Aqr (Ciardi, Howell, & Hauschildt, 1998) we find similar looking accretion regions (size and location) but with clear differences in detail. It appears that changes occur in the accretion regions at all wavelengths but how they are correlated awaits detailed simultaneous, multi-wavelength observations.

7.2. Comparison with Theory

Theoretical models of the coupling region and accretion spot (Wickramasinghe & Meggitt; 1985, Wickramasinghe; 1989, Ferrario et. al.; 1989, Beuermann & Burwitz; 1995, Woelk & Beuermann; 1996 & Harrop-Allin et al.; 1997) indicate that there should be a range of magnetic field lines that capture material, the lighter density regions of the column being grabbed first,

the denser blobs later. The inhomogeneous stream is composed of regions of high (blobby) and low (accretion rain) density blobs. At the coupling region, the low density material is striped off first while the larger blobs penetrate further into the magnetosphere because of their greater ram pressure. The magnetic field of the WD acts like a giant mass spectrometer. This separation of big and small blobs is likely to be preserved as the material proceeds towards the surface of the WD.

The low density component of the stream forms a shock above the surface of the WD and X-rays emanate from the post-shock region of the flow. Roughly one-half of these X-rays are reprocessed in the WD below and emerge as EUV photons. The remainder escape freely with some fraction undergoing Compton scattering in the pre-shock flow (Kylafis & Lamb, 1982). The high density (large blob) part of the stream very likely penetrates the WD surface (King, 1995) forming a shock that is hidden from view below the surface and directly heats the surface area producing EUV photons in a region centered about the dense part of the stream. Stockman and Schmidt (1995) suggested that the vertical extent of the accretion region reported by WSV is caused by Compton scattering within the accretion column. Litchfield (1990) however, modeled blob accretion onto a WD and finds that the localized heating distorts the WD photosphere, locally raising it by about $\sim 0.4\%$, sufficient to effect the light curve. The average height of $0.023 R_{WD}$ we determine for our raised mound accretion regions are comparable with those predicted by Litchfield.

Thus, the accretion region on surface of the WD will probably reflect the structure of the incoming stream leading to an asymmetric, complex footprint. The assumption would be that the low density material would strike nearer the magnetic pole while the denser material would spread farther away from the pole in magnetic latitude primarily in the direction of rotation, but also towards the WD equator (Wickramasinghe et. el., 1991). Our eclipse data for UZ For and HU Aqr require that the spot is small ($< 0.2 R_{WD}$) in rotational longitude. Brightness gradients in the longitudinal direction would result in asymmetric rise and fall phase light curves if the spot size is greater than about $0.2 R_{WD}$ in longitude. The light curves for all six self eclipsing systems (Fig. 5) are symmetric in the rise and fall phase when the accretion region is scanned vertically which rules out any large scale, asymmetric structure extended in longitude.

In principle, high time resolution light curves of eclipse ingress and egress could be used to map out any longitudinal structures within the accretion regions. However, the 2 s duration eclipse profiles in UZ For and HU Aqr show only a handful of EUV photons which are insufficient for this purpose. The broad dip features which occur in the light curves are asymmetric with respect to the EUV mid-phase, and thus provide the evidence for small scale ($< 0.2 R_{WD}$) geometric and physical horizontal structure within the accretion regions.

The high density portion of the accretion stream is likely to be more effective in absorbing or scattering EUV photons than the low density parts. We know that the accretion stream near the coupling region (i.e., the far-field stream) is quite capable of removing EUV flux since we see the evidence in the narrow stream dips that, at times, saturate to zero (in the systems UZ For, EF

Eri, HU Aqr, AN UMa, and V834 Cen). The broad dips, caused by the near-field stream very near the WD surface, never remove all the EUV flux and reach zero. Thus, either the accretion stream near the shock and the WD surface is very ionized and a much less effective photoelectric absorber, or the EUV emitting region is larger than the width of the dense part of the stream and can never be fully occluded by the stream. It is likely that both of these effects are present.

Incorporating the ideas discussed above, we present a scenario that explains the features observed in the EUV light curves, the broad dip / bright phase spectral ratios, and the large tilts of the accretion column required by the column absorber model (§4.3). The schematic diagram in Figure 11 shows an edge-on view of a raised accretion spot ($h = 0.02 R_{WD}$, mildly extended in WD longitude and latitude with an accretion column tilted at a 10° angle away from the magnetic pole in the direction of rotation. The high line density indicates the high density portion of the accretion column where it depresses the otherwise raised accretion region. Thus, for the proper hydrodynamic conditions (Woelk & Beuermann, 1996, King 1995) the shock can become buried below the (raised) WD surface. The white portion corresponds to the hotter regions and is the source of the hardest EUV radiation. The gray portion illustrates the outer, cooler source of the softer EUV. The large tilts required in some instances of our absorber modeling are merely a consequence of using a uniform density accretion column as a first approximation. A model using a non-uniform accretion column can trade large tilt angle for higher density regions within the near-field stream.

The bottom of Figure 11 shows a sequence of pictures that illustrate how such a spot appears when seen rotating across the surface of the WD. The views at different phases illustrate that the column may occlude different regions of the spot during the binary orbit. The system inclination and spot parameters in Figure 11 are those of UZ For, and the three pictures correspond to the rise, broad dip, and bright phases marked as such in Figure 3. Only the dense portion of the accretion column is shown (as a translucent cylinder). The inner portion of the spot (white region) that trails the dense accretion column is the location of the lower density stream impact (greater shock height) with the WD photosphere. Again, this inner region is a major source of the harder EUV radiation while the surrounding outer region is the source of softer EUV radiation.

As the binary rotates, the accretion column will occult different parts of the accretion region. At phases when we look through the dense portion of the stream towards the the hotter, inner region of the accretion spot, we expect this inner region to be more fully obstructed than the cooler, outer region resulting in a broad dip phase with a softer spectrum. This is in fact what we found for our broad dip / bright phase spectral ratios discussed in §5..

The non-absorbed geometric model predicts as much as twice the radiation than was actually seen during the central portions of some of the light curves (see the column labeled “Ratio” in Table 2). What happens to the energy of the radiation that is removed during the various dip phases? If the dips are caused solely by Compton scattering, which is at a maximum when we look parallel to the accretion column, then the radiation simply reappears during the rise and fall

phases when the column presents itself perpendicularly. If the dips are caused by photoelectric absorption, then the excited material impacts the WD surface a few seconds later creating an accretion region that is hotter than it would have been otherwise.

8. Conclusions

We have analyzed EUV light curves for ten AM Her systems. All show strong modulations as a function of orbital phase. Projection effects account for the overall bright and faint phases, but cannot explain the sharp transitions and dips seen in the light curves. In the systems where the accretion spot rotates behind the limb of the WD for some portion of the phase (category 1), the rise and fall phases of the light curve are very steep, and are symmetric about the EUV mid-phase. The observations imply two things: first, the shape of the steep rise and fall phases is dominated by vertical extent of the accretion spot, and second, any longitudinal structure of the accretion region must be less than 0.2 of the R_{WD} , since a larger accretion region would produce an asymmetric lightcurve during the rise and fall phases. For the eclipsing systems UZ For and HU Aqr, the short ingress and egress times directly set upper limits to the spot size of $\leq 0.23 R_{WD}$.

All the light curves show one or more dips. The eclipsing systems constrain the model well and yield the best results for orbital inclination, spot latitude and longitude, spot height, and spot size. Once the viewing geometry is established, the phasing of the dips restricts the spatial location of where the accretion stream material must reside in order to self-eclipse the accretion region. The accretion stream, when it is far from the WD surface, quickly crosses the line of sight to the accretion spot and can completely occlude the spot. These narrow dips last typically < 0.1 of the orbital phase, often saturate to zero flux, and show no wavelength dependence for the absorption. The broad dips typically last ~ 0.25 of the orbit, are asymmetric in profile, occur well before EUV mid phase, never saturate to zero, and show a *softer* spectrum than the non-dip phases. If the accretion column strikes the accretion region normally, and is concentric with the spot, the expected light curve would be symmetric and show a broad dip at phase 0 as predicted by ID83. The large asymmetries present in all the observed AM Her light curves are *direct* evidence for asymmetries within the accretion regions. An elongated spot, with the dense portion of the accretion column eccentrically contacting the spot in the direction of binary rotation can explain the phasing, duration in phase, and depth of the broad dips. Furthermore, if the accretion spot shows a temperature gradient, (hottest towards the center, coolest at the edges), and the column width is less than the EUV emitting area (or has a non-uniform density, or both), the broad dips will never saturate to zero and their spectra will be softer when the dense portion of the column hides the hottest part of the spot.

Using detailed EUV photometric and spectroscopic observations of AM Herculis stars, we have constructed an appropriate model of the accretion regions which include effects of both the far- and near-field accretion stream. Many of our results below apply equally well to observations

of AM Herculis stars in other high energy bandpasses. Summarizing our relevant findings we have:

1. A flat, circular geometric accretion spot model only accounts for the gross features of the EUV light curves, namely the faint phase, the rise to a maximum, and then the return to the faint phase. This model does not match the observations during the steep rise and fall phases (which depart from cosine behavior), for which a vertically extended structure is needed. We have chosen to model this simply as a hemispherical structure, but more complex geometries are possible.
2. All ten stars show large modulations in the form of dips in their EUV light curves that are inconsistent with cosine projection effects. All stars where the accretion region is known to lie in the northern hemisphere (thus guaranteeing that the accretion stream crosses the line of sight to the accretion region) show a far-field stream eclipse of the accretion region. In addition, the two highly inclined systems VV Pup and UZ For, whose spots are in the southern hemisphere, also show evidence for far-field stream eclipses indicating a non-zero width of the coupling region. Eight stars show additional dip features other than what can be accounted for by the far-field stream. The fraction of flux “missing” amounts to as much as 50% of the flux predicted by the non-absorbed geometric model (see Table 2).
3. All AM Herculis stars with multiple EUV observations (UZ For, RE1149, QS Tel, HU Aqr), show significant long term variations in the features of their lightcurves, (eg. the duration of the bright phase, and the depth and position in phase of both the far-field stream dips, and the near-field broad dips). All stars observed also show short term orbit to orbit variations.
4. The cause of a majority of the features of the EUV light curves is highly dependent on viewing geometry (i.e., viewing angle to the spot and through the accretion stream). The remaining variations are due to the physical structure and properties of the accretion stream and near-field column themselves. Attributing the causes of the features in the light curves simply to various astrophysical effects is incorrect until all the geometrical effects have been taken into account and separated from the physical effects.
5. The low inclination systems (category 2) show more complex EUV light curves and dip features, attributable again mainly to geometric aspects of both the accretion stream and the near-field column. The additional complexity observed in these stars is probably caused by the fact that the angle subtended between the spot normal and the viewing direction is small and the accretion region is viewed nearly face on, through a long length of the column, for a large fraction of the binary phase ($\sim 25\%$). The accretion region in AM Her is seen nearly face-on as it crosses the central meridian which (along with its rather weak magnetic field) may account for it possessing the most complex lightcurve of the category 1 systems.
6. Our geometric model matches the EUV observations of the AM Hers very well and yields spot sizes averaging $0.06 R_{WD}$, or $f \sim 1 \times 10^{-3}$ the WD surface area, and average accretion

spot heights around $0.023 R_{WD}$. When the accretion spot undergoes self eclipse (category 1 systems) the raised mound model is useful for determining the system inclination to within 5 degrees, and the spot colatitude to within $7\text{--}15^\circ$. The near perfect symmetry of the rise and fall phase of the six systems shown in Figure 5 preclude any large scale ($> 0.2 R_{WD}$) structure of the accretion region. The height of the accretion region above the WD surface seems to be correlated with overall EUV flux (accretion rate), but the spot longitude ψ does not (see Table 2).

7. All category 1 light curves show a small amount of EUV flux from above the accretion region. This flux can be isolated and observed during the short phase intervals when the main accretion region itself is just hidden from view behind the WD limb. The EUV spectra during these phases show no emission lines characteristic of a high temperature, corona-like plasma, but signal-to-noise available during these short phases is insufficient to completely exclude the possibility of weak emission features. Preliminary analysis of high signal to noise EUV spectra of the highly magnetic system AR UMa (Howell & Sirk, 1998) observed during outburst show no evidence of emission lines at any phase. This result adds weight to the growing body of negative evidence against the existence of a high temperature, low density plasma (corona) surrounding the accretion regions of AM Her stars.
8. The far-field accretion stream causes narrow dips in the light curves that saturate to zero in 5 systems: UZ For, AN UMa, EF Eri, V834 Cen, and HU Aqr, and reduce the flux by a factor of 2 for VV Pup. The spectra extracted for UZ For and VV Pup during these narrow dip phases show no wavelength dependent variations or absorption features (lines or edges) compared with spectra obtained during the out-of-dip phases. Thus, in at least these two systems, the far-field accretion stream behaves like a grey absorber.
9. A broad dip occurs at binary rotation phases where the far-field accretion stream is not interfering with our view to the accretion region. In addition, the broad dips do *not* occur at EUV phase zero as predicted by assuming a circular spot impinged normally by a cylindrical accretion column (ID83). The cause for these broad dips must be from material very near the WD surface and appears to be almost entirely caused by Compton scattering. The broad dips tell us that either the column is highly inclined with respect to the WD surface, non-uniform in nature, or the source of maximum EUV radiation is not concentric with the densest portion of accretion column. Since polarimetry data show that the magnetic field is only slightly tilted with respect to the spot normal in several AM Her stars (Meggitt & Wickramasinghe, 1989), we are forced to conclude that the broad dips are caused by small scale ($< 0.2 R_{WD}$) asymmetric structure in both the accretion spot and the near-field column.
10. The broad dip / bright phase spectral ratio shows a wavelength dependence in that the broad dip phase spectra appear softer than the bright phase spectra. Absorption by a cold absorber (neutral hydrogen) is not possible due to the high state of, or complete ionization of

H and He and would give a very different spectral slope. It thus appears that the broad dips are caused by some (unequal) combination of a warm absorber, Compton scattering, and geometric effects caused by the near-field stream. It is apparent that near the WD surface, the accretion column and region have a highly asymmetric structure which can significantly change on short timescales, days (WSV) to months and longer (see Fig 10, and Sirk et al., 1998).

We have detailed the geometric nature of AM Herculis accretion regions via the use of high-quality EUV photometric and spectroscopic observations. Our few-component model provides good fits to the data, but also indicates some areas where a more complex structure is present. The magnetic field strength of the WD and the mass accretion rate are likely to be the dominant mechanisms which cause both the general similarities observed in many of the AM Hers, as well as the detailed differences between systems. The next step in understanding the details presented here is to use the presented model, along with the appropriate physical conditions likely to be present within the stream and accretion region itself, to confirm our results. We need to understand the roles played by geometry, Compton scattering, photoelectric absorption, magnetic field strength, mass accretion rate, and other physical properties, in order to form a better picture of the accretion regions in AM Hers.

The authors wish to thank the staff of the Center for Extreme Ultraviolet Astrophysics for their help throughout the EUVE mission. SBH and MMS wish to acknowledge partial support of this research by NASA EUVE grants NAG 5-3523 & 5-4241 and NASA ADP grants 5-2989 & 5-3379. MMS extends thanks to Patrick Sirk for Figure 11. Adrienne Cool provided many useful comments on an early version of the manuscript. Mark Cropper and Axel Schwope have also contributed useful comments. This manuscript is certified Cruelty Free; no graduate students were abused in its preparation. Not dishwasher safe.

Table 1. Observation Log

System	Instrument ^a	Starting Time (GMT)	Duration (hours)	Exposure (ks)	N Orbits ^b	Mean Countrate ^c (s ⁻¹)
UZ For	ScB	1993 Oct 16 04:58	73	98	13	0.37
UZ For	DS	1993 Nov 18 18:47	78	85	11	0.93
UZ For	DS	1995 Jan 15 20:34	90	82	11	0.82
VV Pup	DS	1993 Feb 07 21:25	34	37	6	1.53
AM Her	DS	1993 Sep 23 17:57	114	123	11	2.97
RE1149+28	DS	1993 Feb 22 18:50	53	64	12	0.48
RE1149+28	ScA	1994 Mar 08 01:56	117	147	27	0.26
RE1149+28	DS	1994 Dec 26 06:06	198	145	27	0.15
HU Aqr	DS	1996 May 29 02:13	123	121	16	0.044
RE1844-74	DS	1994 Aug 17 13:53	154	188	35	0.65
EF Eri	DS	1993 Sep 05 13:42	99	107	22	0.69
AN UMa	DS	1993 Feb 27 22:14	27	33	5	0.32
V834 Cen	DS	1993 May 28 03:07	35	37	6	0.76
QS Tel	DS	1993 Oct 06 07:51	105	113	13	1.55

^aDeep Survey (DS), Scanner A (ScA), and Scanner B (ScB).

^bNumber of full binary orbits sampled.

^cThe Scanner countrates have been multiplied by a factor of 2.2 to account for their smaller effective area compared with that of the the Deep Survey in the Lexan/Boron passband (Sirk et. al., 1997).

Table 2. System Parameter Fits

The system inclination is ι . The angle between the rotational pole and the EUV accretion spot is β . The radius and the height of the accretion spot are r and h , respectively, in units of R_{WD} . The maximum height of the accretion column above the WD surface that shows significant flux is h_{col} in units of R_{WD} . The longitude of the accretion spot is ψ , the field strength of the primary magnetic pole is B . The final columns list the ratio of the absorber model flux to the un-absorbed model, and the absorption coefficient τ found from the absorber model. Italic entries for ι , β , r , h , and h_{col} are the parameter solutions derived from our geometric model fits (roman entries indicate fixed parameters). Italic entries for values of the period and ψ are determined from *EUVE* data. Non-derived entries (roman) are from Cropper (1990), except where noted.

System	Inst.	Date	Period min	ι ($^{\circ}$)	β ($^{\circ}$)	r (R_{WD})	h (R_{WD})	h_{col} (R_{WD})	ψ ($^{\circ}$)	B (MG)	Ratio	τ
UZ For	ScB	Oct 93	126.5	80.2	<i>114.1</i>	<i>.073</i>	<i>.018</i>	<i>.14</i>	<i>55</i>	56	<i>0.47</i>	<i>22</i>
UZ For	DS	Nov 93	126.5	<i>80.2</i>	<i>136.6</i>	<i>.060</i>	<i>.031</i>	<i>.15</i>	<i>49</i>	56	<i>0.61</i>	<i>23</i>
UZ For	DS	Jan 95	126.5	<i>81.7</i>	<i>136.5</i>	<i>.045</i>	<i>.021</i>	<i>.15</i>	<i>49</i>	56	<i>0.61</i>	<i>23</i>
VV Pup	DS	Feb 93	100.4	<i>73.1</i>	<i>147</i>	<i>.022</i>	<i>.011</i>	<i>.12</i>	49	32	<i>0.65</i>	<i>50</i>
AM Her	DS	Sep 93	185.6	<i>37.1</i>	<i>68</i>	<i>.045</i>	<i>.013</i>	<i>.033</i>	31	12	<i>0.62</i>	<i>35</i>
RE1149+28	DS	Feb 93	<i>90.17</i>	<i>70</i>	<i>142</i>	<i>.10</i>	<i>.035</i>	<i>.12</i>	—	43 ^a	<i>0.89</i>	<i>11</i>
RE1149+28	ScA	Mar 94	<i>90.17</i>	<i>70</i>	<i>136</i>	<i>.054</i>	<i>.025</i>	<i>.12</i>	—	43 ^a	<i>0.78</i>	<i>29</i>
RE1149+28	DS	Dec 94	<i>90.17</i>	<i>70</i>	<i>143</i>	<i>.10</i>	<i>.030</i>	<i>.12</i>	—	43 ^a	<i>0.86</i>	<i>27</i>
HU Aqr	DS	May 96	125.0	<i>81</i>	<i>40</i>	<i>.036</i>	<i>.021</i>	<i>.10</i>	<i>49</i>	37 ^b	—	—
RE1844–74	DS	Aug 94	90.10	<i>73</i>	<i>144</i>	<i>.090</i>	<i>.025</i>	<i>.12</i>	—	10 ^c	<i>0.94</i>	<i>8</i>
EF Eri	DS	Sep 93	81.01	<i>52</i>	<i>33</i>	<i>.059</i>	<i>.025</i>	—	—	11 ^d	—	<i>12</i>

^aSchwope, A. D., 1997, private communication

^bSchwope et. al., (1993)

^cRamsay et. al., (1996)

^dPaerels, F., 1995, private communication

Table 3. System Geometry Comparison

System	Present Work		Polarimetry		Ref.	Spectrophotometry		Ref.
	ι	β	ι	β		ι	β	
UZ For	81 (2)	136 (5)	81 (2)	150 (12)	1	85 (3)	155	2,3
HU Aqr	81 (5)	40 (10)	80 (5)	40 (10)	4	83 (3)	—	5
VV Pup	73 (3)	147 (5)	74	147	6			
AM Her	37 (4)	68 (8)	52	49	7			
RE1844–74	73 (5)	144 (7)	60	167	8			
EF Eri	52 (5)	33 (10)	55	35	6			

Numbers in parentheses are the 1σ errors. 1)From optical eclipse analysis by Bailey & Cropper, (1991). 2)Beuermann, Thomas & Schwope, (1988). 3)Schwope, Beuermann & Thomas, (1990). 4)Glenn et. al., (1994). 5)Schwope, Mantel & Horne, (1997). 6)Meggitt & Wickramasinghe, (1989). 7)Wickramasinghe et al., (1991). 8)Bailey et. al., (1995).

REFERENCES

- Bailey, J. & Cropper, M. 1991, MNRAS 253, 27
- Bailey, J., Ferrario, L., Wickramasinghe, D., Buckley, D & Hough, J., 1995, MNRAS, 272, 579.
- Beuermann, K. & Schwöpe, A. D., 1994, ASP Conf. Proc, 56, ed. A. W. Shafter, 119
- Beuermann, K. & Burwitz, V., 1995, ASP Conf. Proc. 85, Cape Workshop on Magnetic Cataclysmic Variables, ed. D. A. H. Buckley & B. Warner (San Francisco: ASP), 99
- Bowyer, S. & Malina, R. F., 1991 in Extreme Ultraviolet Astronomy, ed. R.F. Malina and S. Bowyer, (New York: Pergamon Press), 397
- Boyd, W., Jelinsky, P., Finley, D. F., Dupuis, J., Abbott, M., Christian, C. A., & Malina, R. F., 1994 in “EUV, X-Ray, and Gamma-Ray Instrumentation for Astronomy V,” Proc. SPIE, 2280, 280-296.
- Cameron, A.G.W. & Mock, M., 1967, Nature, 215, 464
- Ciardi, D., Howell, S. B., & Hauschildt, P., 1998, ApJ, submitted
- Cropper, M.S., 1990, Sp. Sci. Rev., 54, 195
- Cropper, M., Ramsey, G., & Wu, K., 1997, MNRAS, in press.
- Craig, N., Abbott, M., Finley, D., Jessop, H., Howell, S., B., Mathioudakis, M., Sommers, J., Vallerger, J., & Malina, R., 1997, ApJ Suppl., 113, 131.
- Ferrario, L., Wickramasinghe, D.T. & Tuohy, I. R. 1989, ApJ., 341, 227.
- Harrop-Allin M. K., Hakala, P., Cropper, M., Hellier, C., & Ramseyer, T., 1997, in prep.
- Howell, S. B., Sirk, M., Ramsey, G., Cropper, M., Potter, S., and Rosen, S., 1997, ApJ, 485, 333.
- Howell, S. B., Sirk, M. M., Malina, R. F., Mittaz, J. P. D., & Mason, K.O., ApJ, 439, 991, 1995
- Howell, S. B., Sirk, M. M., 1998, in prep.
- Hurwitz, M., Sirk, M.M., Bowyer, S. & Ko, Y.-K., 1997, ApJ, 477, 390
- Imamura, J. N. & Durisen, D. H. 1983, ApJ, 268, 291 (ID83).
- King A.R. & Williams, G.A., 1985, Mon. Not. R. Astro. Soc., 215.
- King, A. R., 1995, ASP Conf. Proc. 85, Cape Workshop on Magnetic Cataclysmic Variables, ed. D. A. H. Buckley & B. Warner (San Francisco: ASP), 21
- Kuijpers, J. & Pringle, J.E., 1982, A & A, 114, L4
- Kylafis, N. D. & Lamb, D. Q., 1982, Ap. J. Suppl., 48, 239.
- Lamb, D. Q. & Masters, A. R., 1979, ApJ, 234, L117
- Litchfield, S. J., 1990 in “Accretion–Powered Compact Binaries”, ed. C. Mauche, Cambridge Press, p.339.

- Liebert, J. & Stockman, H.S., (1985), in “Cataclysmic Variables and Low Mass X ray Binaries”, eds. D.Q. Lamb & J. Patterson, Reidel, Dordrecht, p. 151.
- Mason, K. O., 1985 Sp. Sci. Rev., 40, 99.
- McDonald, K., Craig, N., Sirk, M. M., Drake, J. J., Fruscione, A., Vallergera, J. V. & Malina, R. F., 1994, *Astron. J.*, 108, 1843-1853
- Meggitt, S.M.A. & Wickramasinghe, D. T., 1989, *MNRAS*, 236, 31.
- Paerels, F., Hur, M. Y., Mauche, C. W., & Heise, J., 1996, *ApJ*, 464, 884.
- Potter, S. B., Hakala, P. J., and Cropper, M., 1998, *MNRAS*, submitted.
- Pringle, J. E., 1981, *ARAA*, 19, 137
- Ramsay, G., Mason, K.O., Cropper, M. Watson, M.G. & Clayton, K. L., 1994, *MNRAS*, 270, 692.
- Ramsay, G., Cropper, M., Wu, K. & Potter, S., 1996, *MNRAS*, 282, 726.
- Rosen, S. R., Mittaz, J.P.D., Buckley, D.A.H., Layden, A. C., Clayton, K.L., McCain, C., Wynn, G.A., Sirk, M.M., Osborne, J.P., & Watson, M. G., 1996, *MNRAS*, 280, 1121.
- Schwope, A.D., 1995, *RvMA* 8, 125S.
- Schwope, A.D., Mantel, K.-H. & Horne, K., 1997, *A & A*. 319, 894.
- Schwope, A.D., Beuermann, K. & Thomas, H.-C., 1990, *A & A*. 230, 120.
- Schwope, A.D., Thomas, H.-C. & Beuermann, K., 1993, *A & A*. 271L, 25.
- Schwope, A. D., et. al., 1998, in prep.
- Sirk, M. M., & Howell, S. B., 1996, in “Astrophysics in the Extreme Ultraviolet”, eds., Bowyer & Malina, Kluwar, p. 343.
- Sirk, M.M., Vallergera, J.V., Finley, D.S., Jelinsky, P. & Malina, R.F., 1997, *ApJ. Suppl.* 110, 347.
- Sirk, M.M., Schwope, A. D., Howell, S. B., Harrop-Allin, M. K., & Cropper, M. 1998, in prep.
- Stockman, H. S., Schmidt, G., Liebert, J., & Holberg, J. 1994, *ApJ*, 430, 323.
- Stockman, H. S., Schmidt, G. D., 1995, *ApJ*, 468, 883
- Vennes, S., Szkody, P., Sion, E. M. & Long, K., 1995, *ApJ*, 445, 921
- Warner, B., 1995, “Cataclysmic Variable Stars”, Chp. 6, Cambridge U. Press.
- Warren, J. K., Sirk, M.M., & Vallergera, J.V., 1995, *ApJ*, 445, 909-920 (WSV).
- Wickramasinghe, D. T., Ferrario, L. & Bailey, J., 1989, *ApJ*, 342, 35.
- Wickramasinghe, D. T. & Meggitt, S.M.A., 1985, *MNRAS*, 216, 857.
- Wickramasinghe, D. T., Bailey, J., Meggitt, S.M.A., Ferrario, L., Hough, J. & Tuohy, I. R., 1991, *MNRAS*, 251, 28.
- Wu, K. & Wickramasinghe, D. T., 1992, *MNRAS*, 256, 329

Woelk, U. & Beuermann, K., 1996, *A & A*, 306, 232.

Fig. 1.— Schematic diagram showing AM Her star viewing geometry. The system inclination is ι , and β is the accretion spot colatitude measured from the rotational pole tilted towards the observer.

Fig. 2.— Geometrical spot model atlas contrasting a flat spot (dashed line) and raised spot (solid line) for four different inclinations ($\iota = 80, 60, 40,$ and 20°), and a range of spot latitudes that span both hemispheres. The spot radius is $0.065 R_{WD}$, and for the raised mound model, the height is $0.03 R_{WD}$ above the WD surface. All plots are normalized to the maximum brightness when the spot normal is pointed directly towards the observer. In all cases, the duration of the bright phase is longer for the raised mound model. For the higher inclination cases ($\iota = 80^\circ$ and 60°) the rise and fall phase is often steeper for the raised mound model than for the flat spot.

Fig. 3.— Phase folded mean light curve for UZ For from 1995 January covering 11 full binary orbits binned at 25 s resolution. Note that the stellar eclipse is total, and the stream dip also briefly saturates to zero flux. The phases marked “Rise” and “Fall” are nearly linear, and very steep in slope. The remaining phases are discussed in the text.

Fig. 4.— Phase folded mean light curves. The six systems where the accretion regions undergo self eclipse (category 1) are shown in the first eight panels, and the remaining four panels show the systems where the accretion region remains visible at all binary phases (category 2). Also shown are the geometric model fits (dotted line), and absorber model fits (solid line). Open symbols denote data points omitted from the fits. The model fitting is discussed in the text. The mean 1σ uncertainty in countrate of all the plotted data points is indicated at the lower right for each light curve. The small inset in each plot represents the WD and shows the location of the accretion region on the central meridian at phase zero for the denoted inclination and spot colatitude.

Fig. 5.— Enlargement of the EUV rise and fall phases for the six category 1 AM Her systems shown in Figure 2. The fall phase is mirror reflected about EUV mid-phase (zero) and shows the near perfect symmetry of the rise and fall phases when the accretion regions are seen at oblique angles (edge-on).

Fig. 6.— Model fits to the fall phase of UZ For contrasting the flat spot (top), raised mound (middle), and raised mound with luminous accretion column models (bottom).

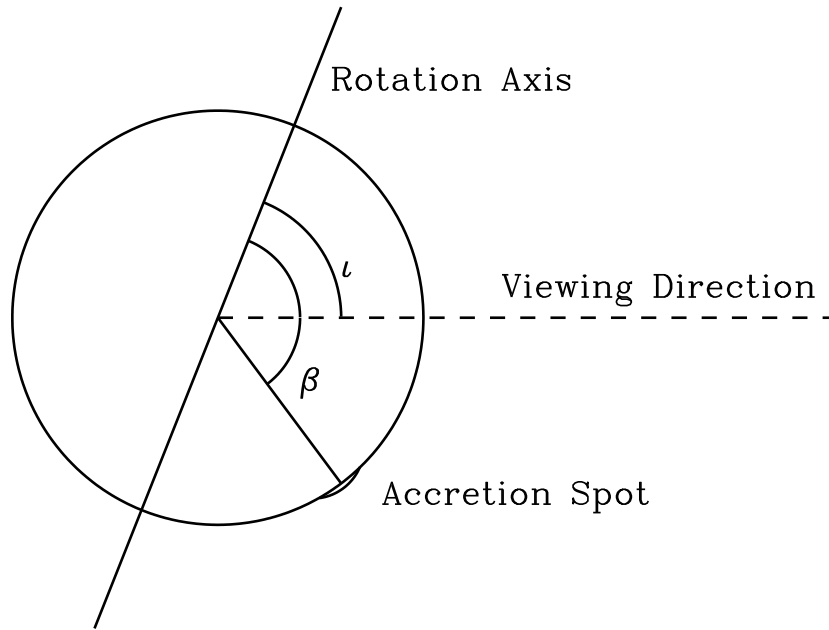
Fig. 7.— Accretion column brightness as a function of height above WD surface for the six self eclipsing systems of Figure 4.

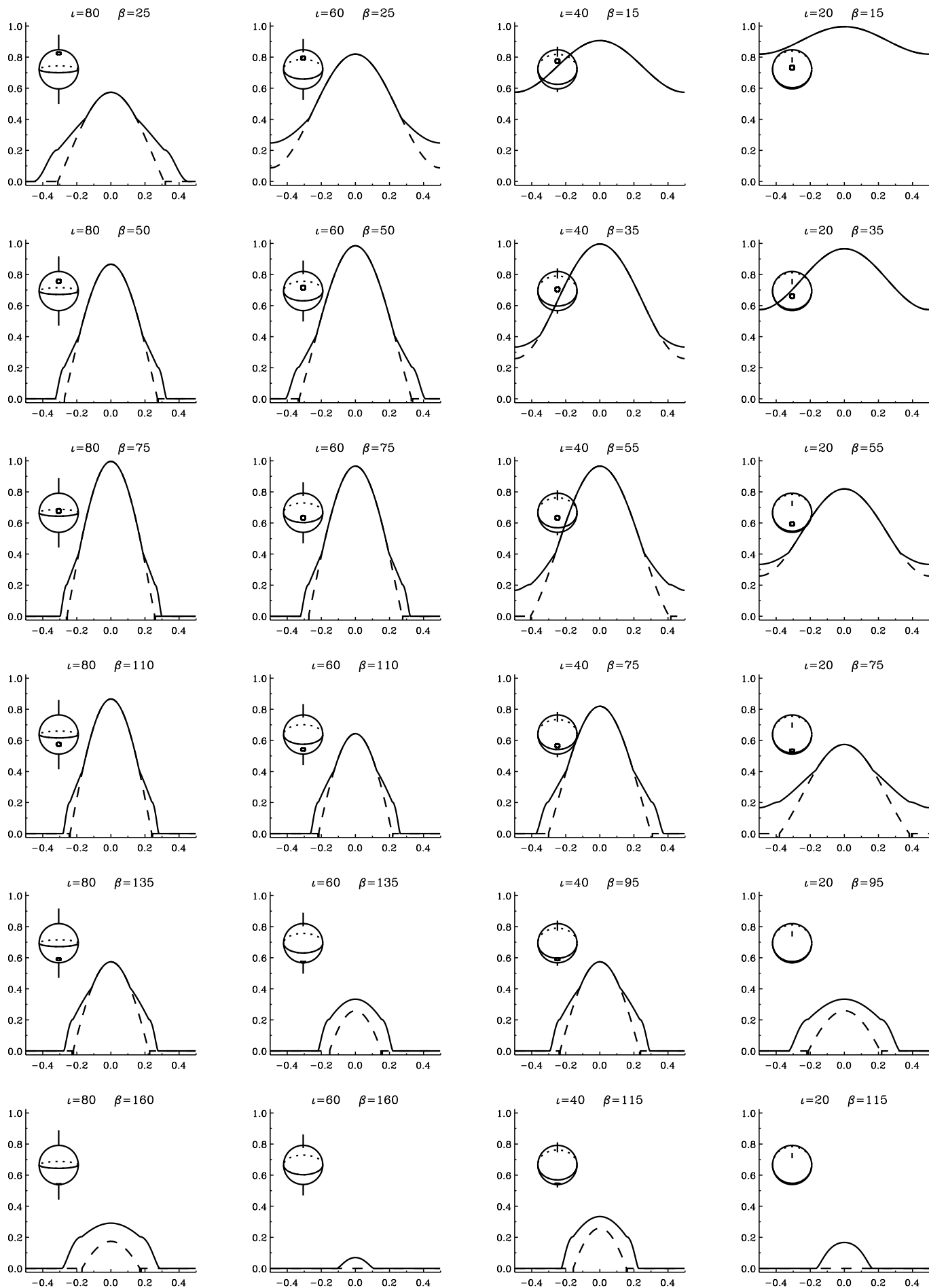
Fig. 8.— Schematic geometry of the accretion column absorber model. The spot radius is r , spot height h , and the angle the accretion column makes with the spot normal in the latitude direction is α . For a given viewing direction, the total absorption is calculated by integrating over all possible path lengths (dotted lines) through the accretion column to the spot.

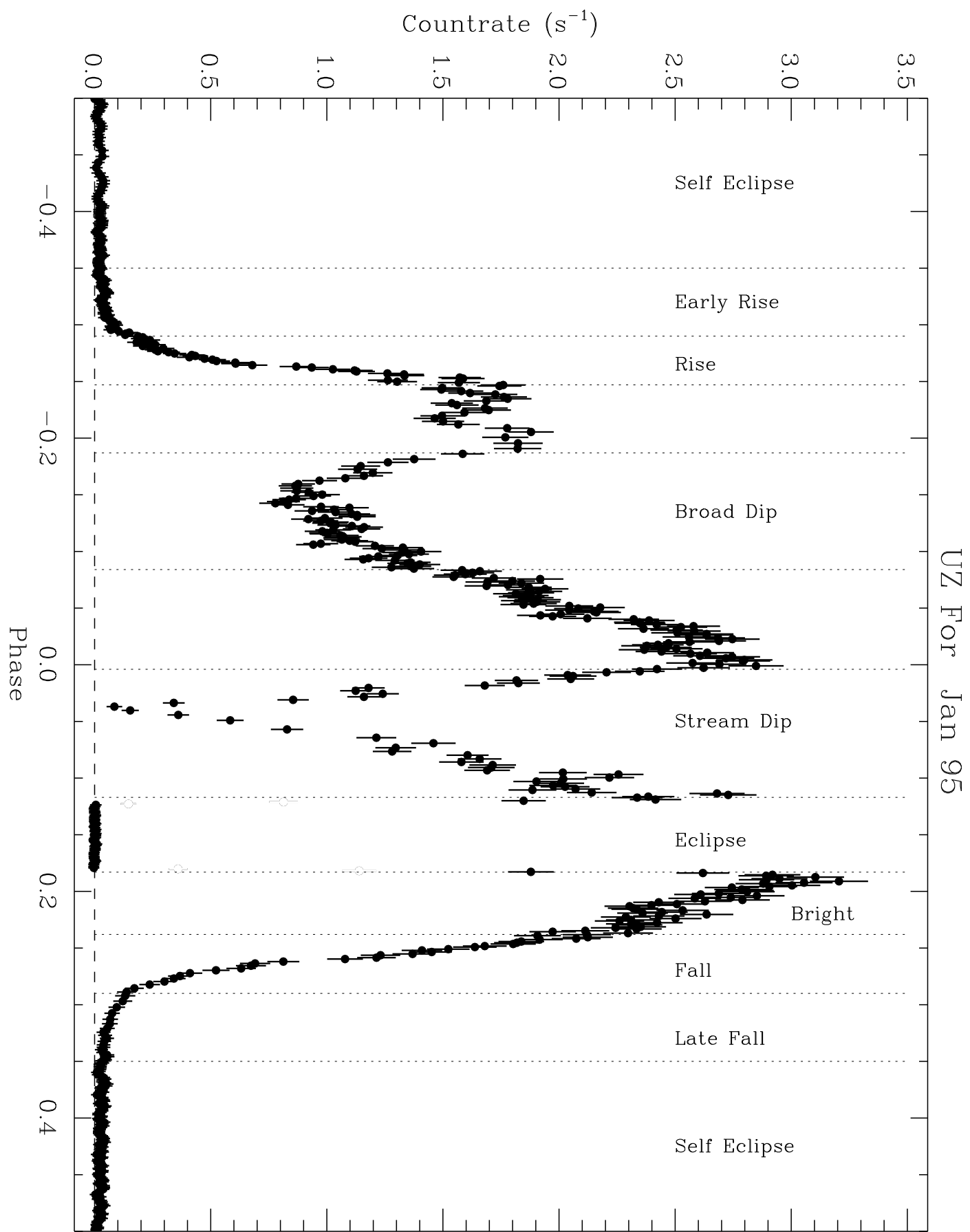
Fig. 9.— Phase-resolved spectra for the bright phase (solid lines), and broad dip phases (dashed lines) for the three EUV bright AM Her systems (upper panels). Lower panels plot the ratio of the broad dip to the bright phase spectra with the thinner lines indicating the one sigma error in the ratio. Least squares linear fits to each ratio (plotted as dashed lines) show slopes significantly greater than zero by 12, 32, and 13 σ for VV Pup, AM Her, and UZ For, respectively, which clearly indicate softer broad-dip phase spectra.

Fig. 10.— Phase folded EUV light curves for UZ For and RE1149+28 showing long term changes in accretion morphology. The spot longitude, the near-field broad dips, and the far-field narrow accretion stream dips all change in depth and phase. The total duration in phase of detectable flux also changes. The light curves are normalized to the brightest observation for each star (solid lines, see also Table 1).

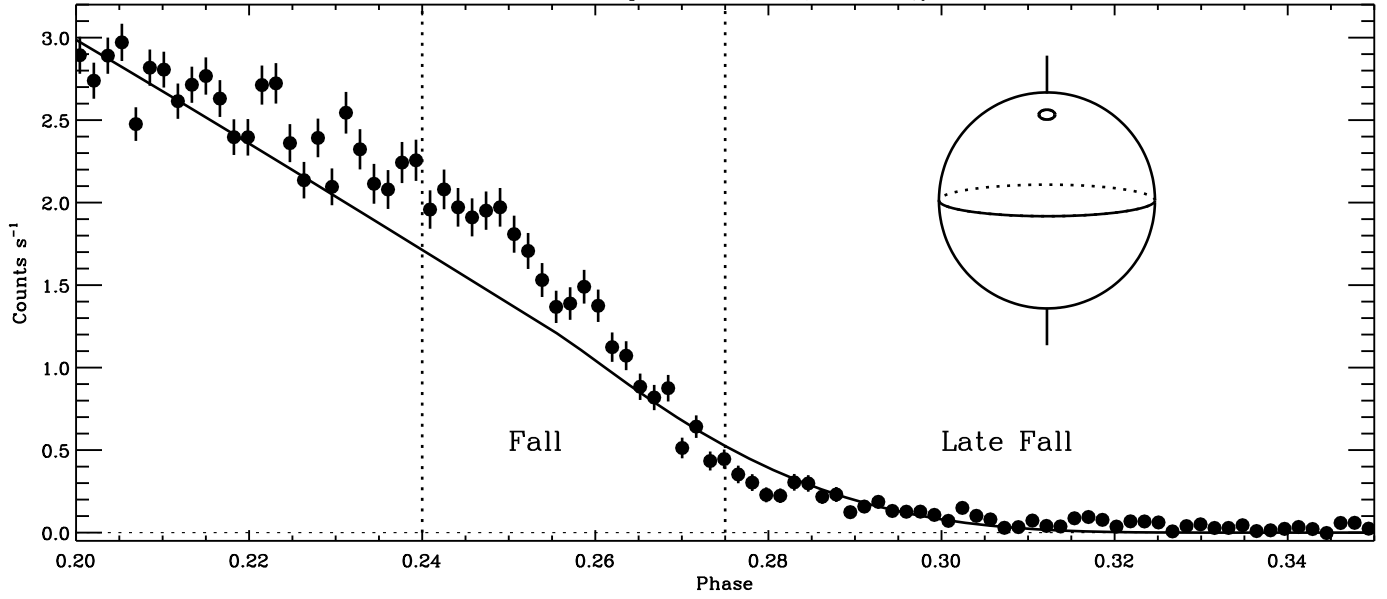
Fig. 11.— (top panel) Schematic diagram showing an edge view of a raised accretion spot with accretion column tilted 10° away from the magnetic pole. The densest portion of the stream, indicated by high line density, is offset from the center of the spot in the direction away from the magnetic pole. (lower panels) The bottom of this figure shows three views of the raised accretion spot extended in the direction of WD longitude and latitude corresponding to the rise phase, broad dip phase, and EUV maximum phase. The model presented here has used the binary inclination and accretion spot latitude ($\iota = 81^\circ$, $\beta = 135^\circ$) of UZ For. Harder emission (white) arises from central portion of the accretion spot and is mostly hidden by the column during the broad dip phase. Softer emission (gray) is visible at all phases.



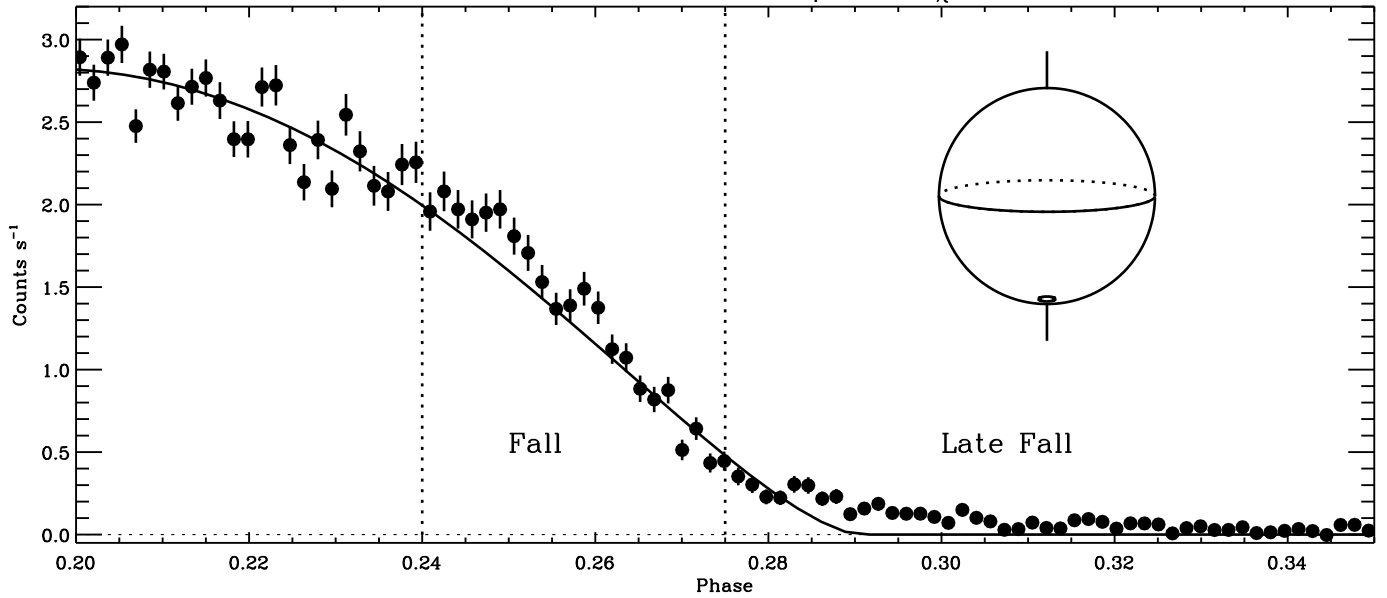




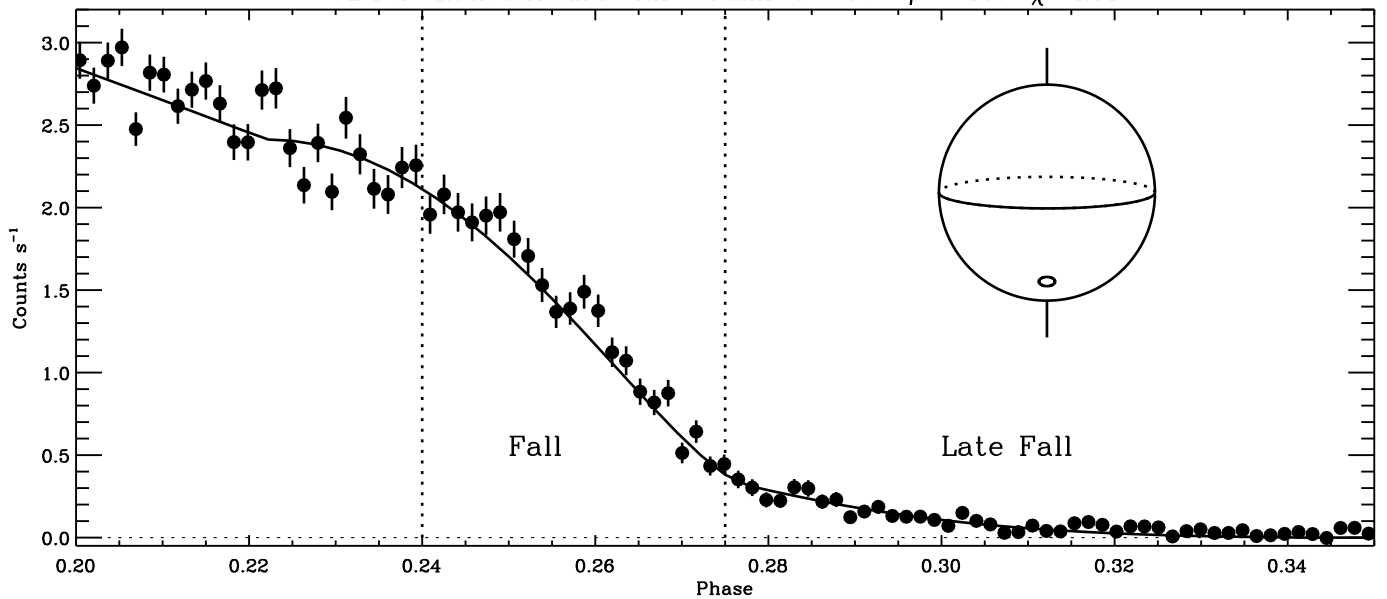
UZ For Flat Spot $\iota = 82$ $\beta = 29$ $\chi^2=4.17$

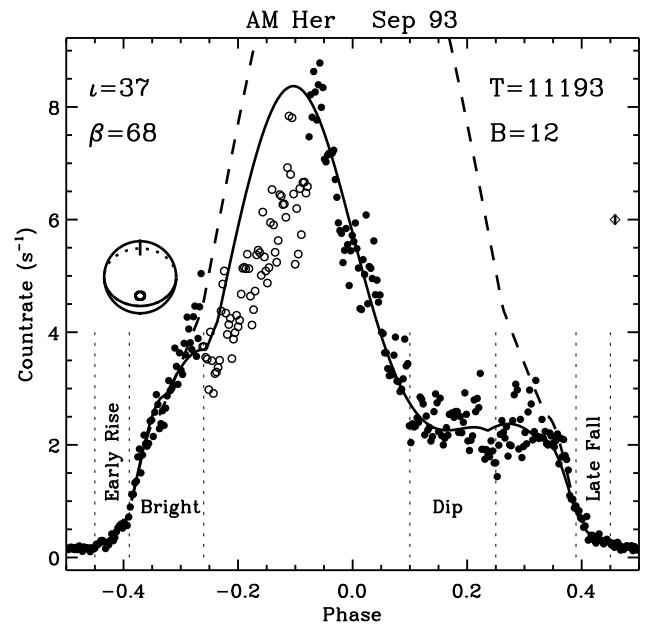
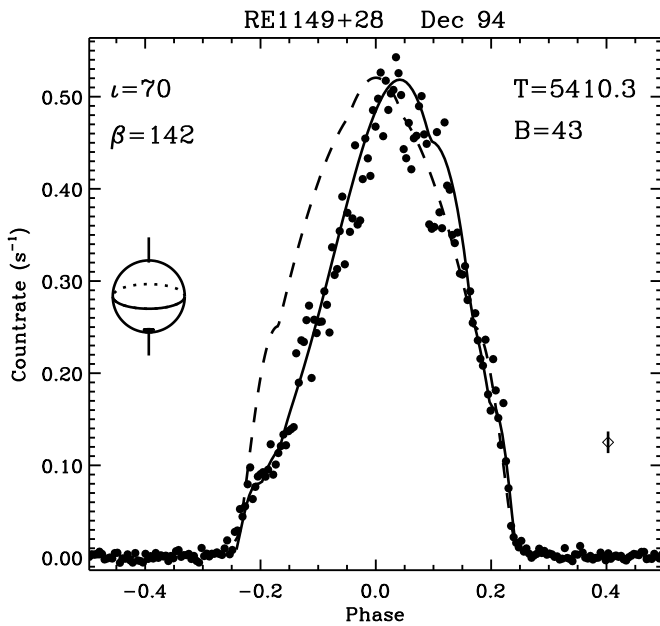
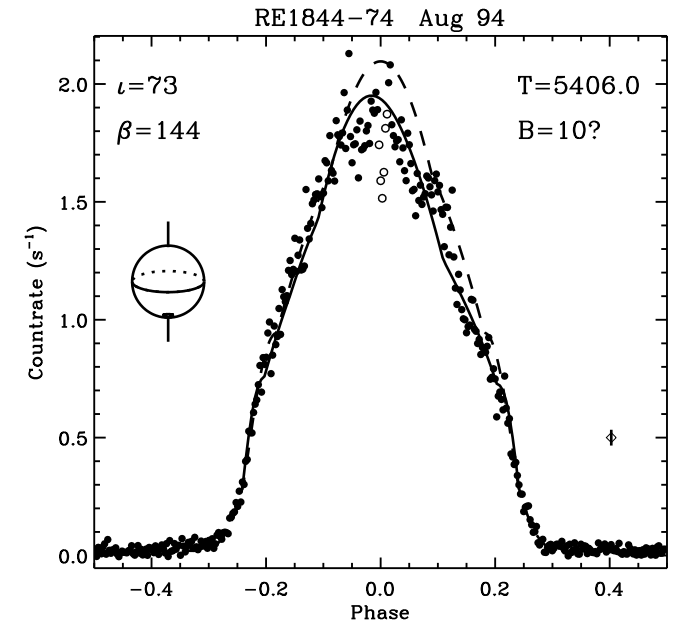
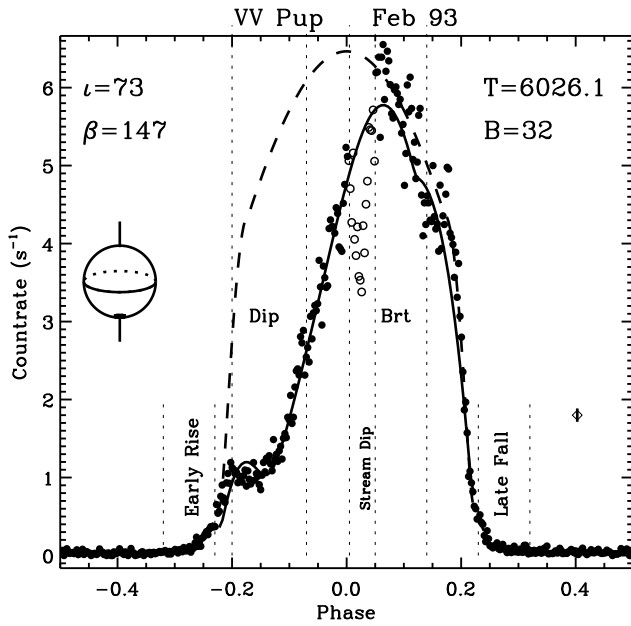
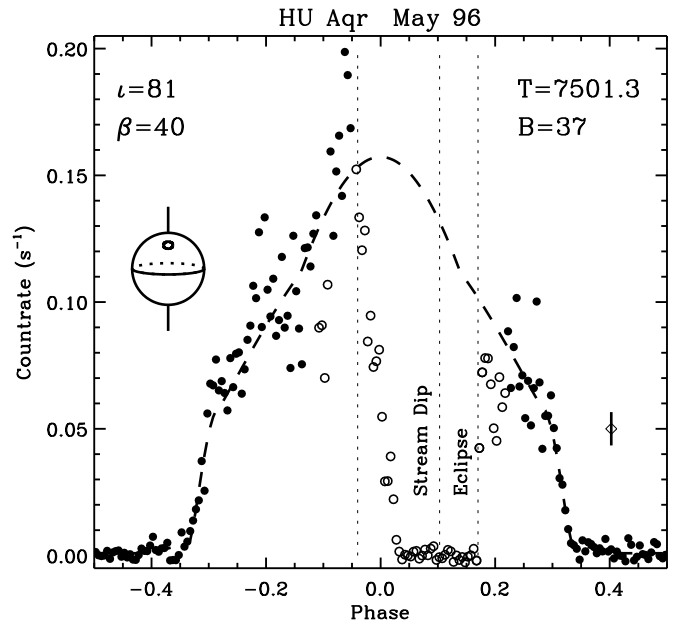
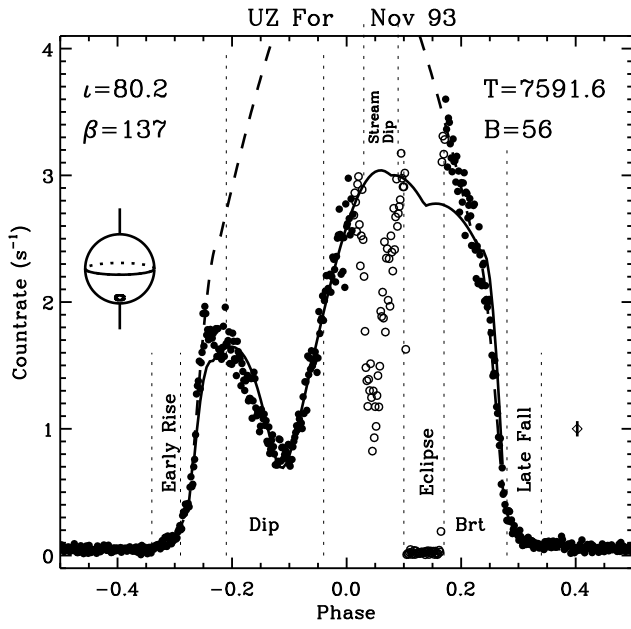


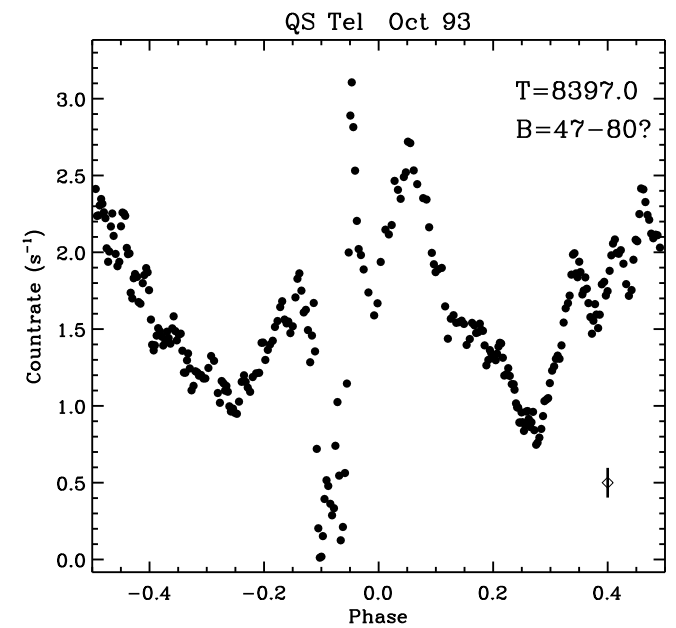
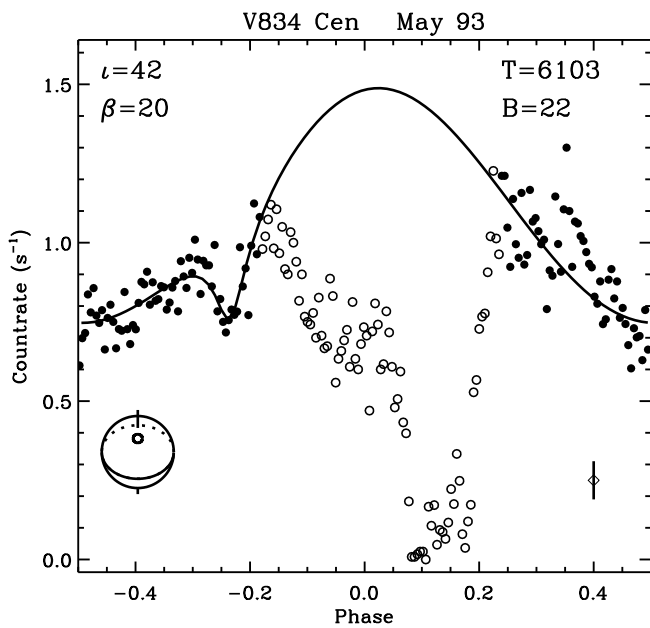
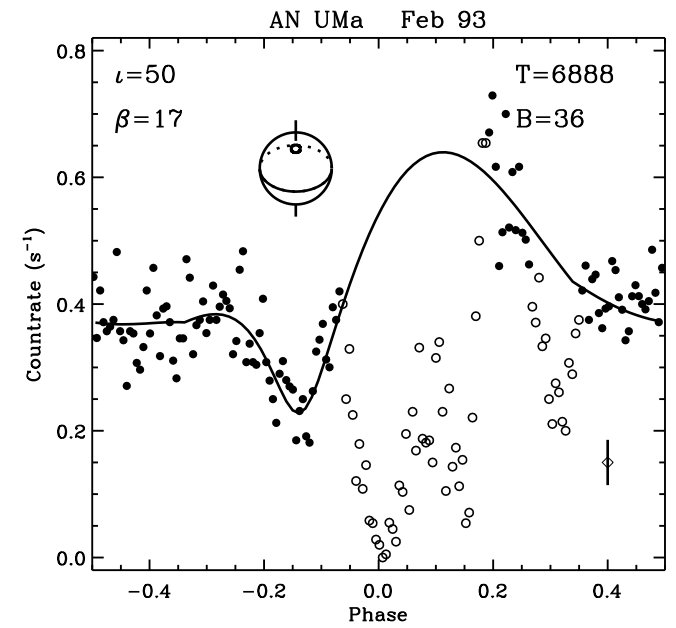
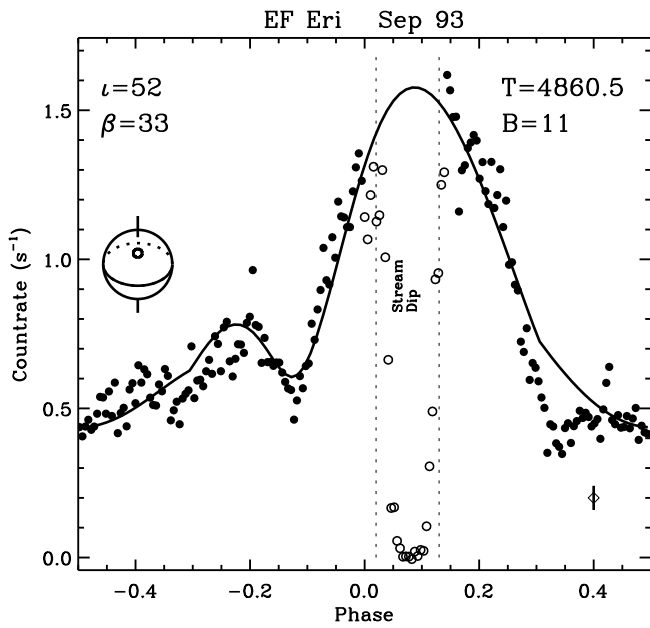
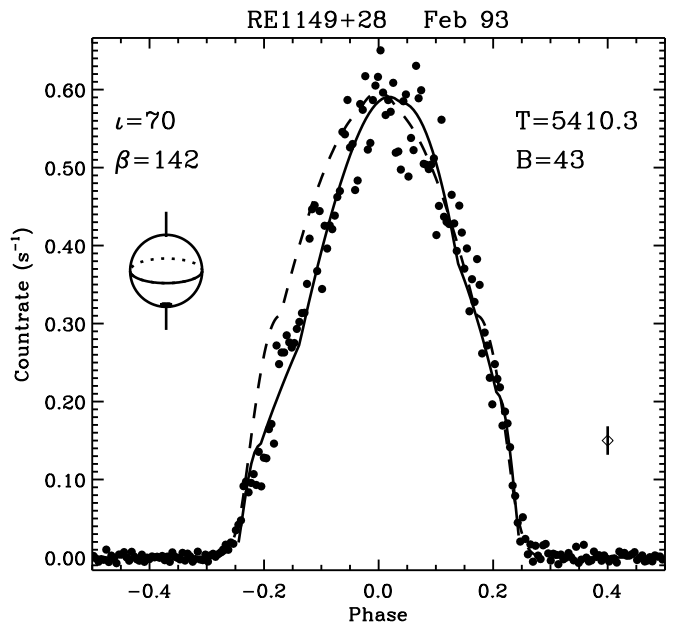
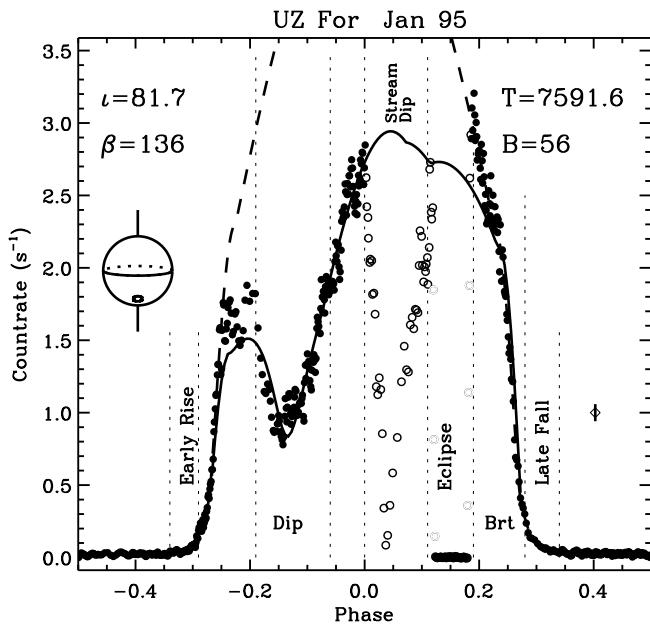
UZ For Raised Mound $\iota = 81$ $\beta = 154$ $\chi^2=3.22$

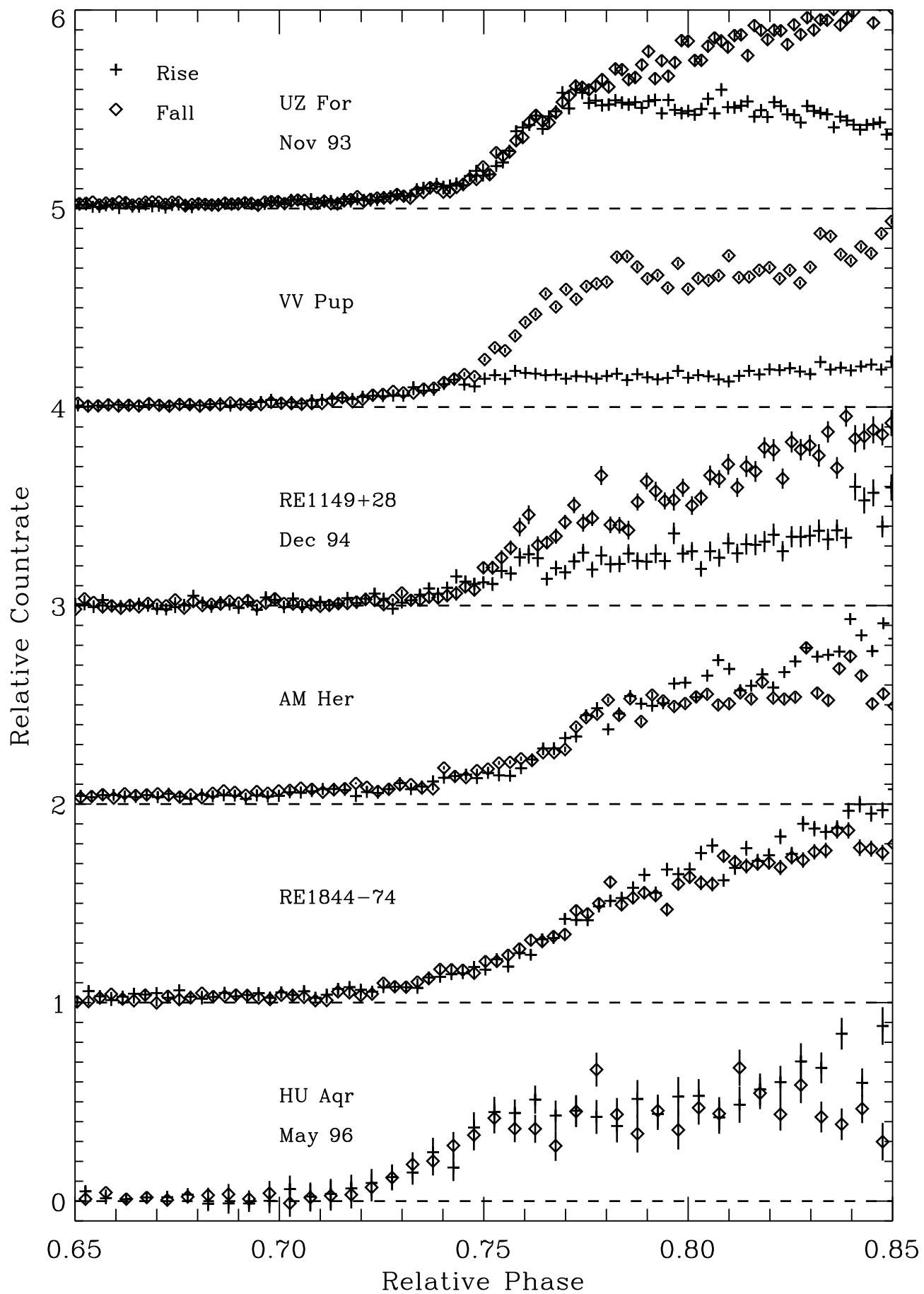


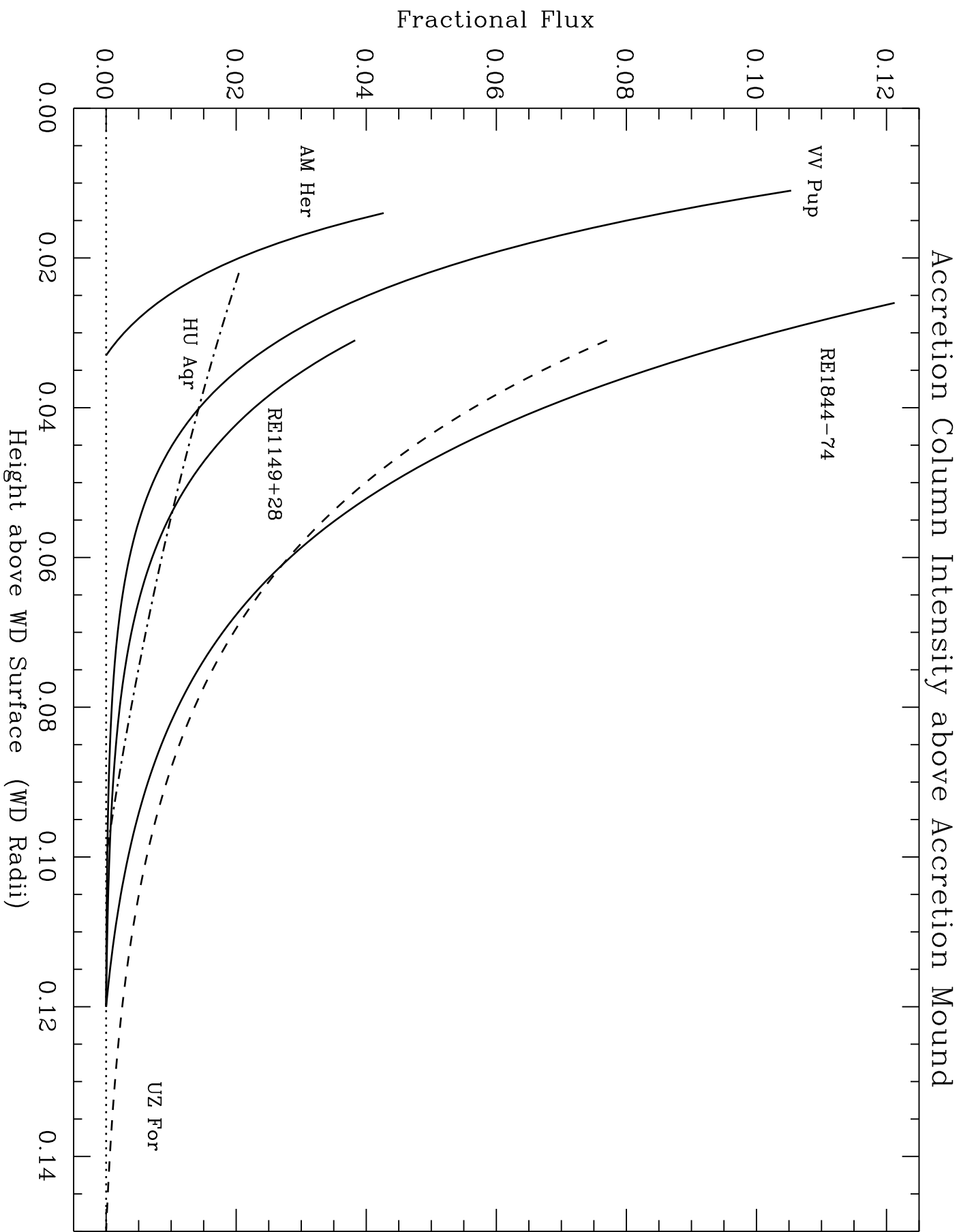
UZ For Rasied Mound with Column $\iota = 80$ $\beta = 136$ $\chi^2=2.81$

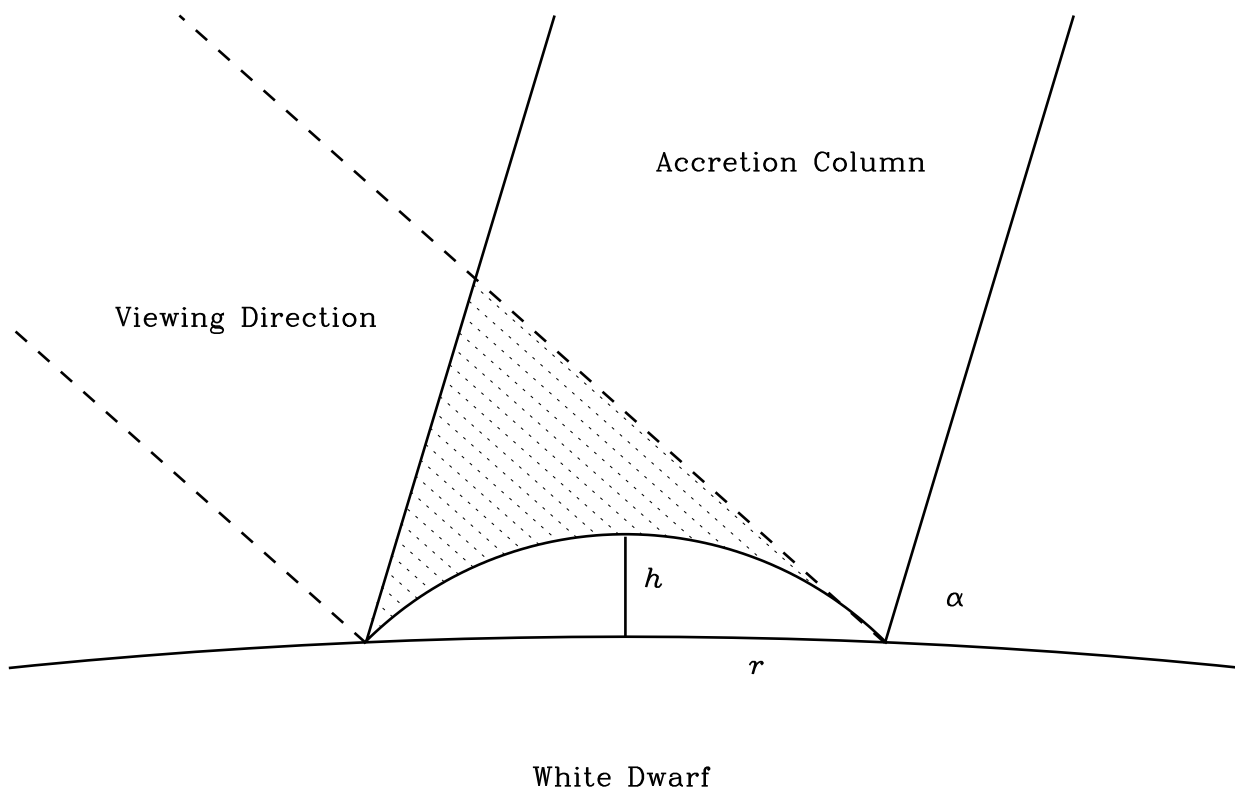


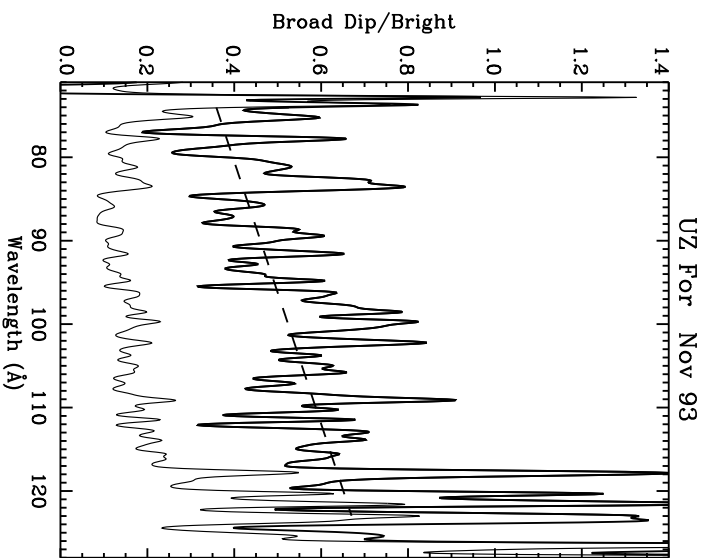
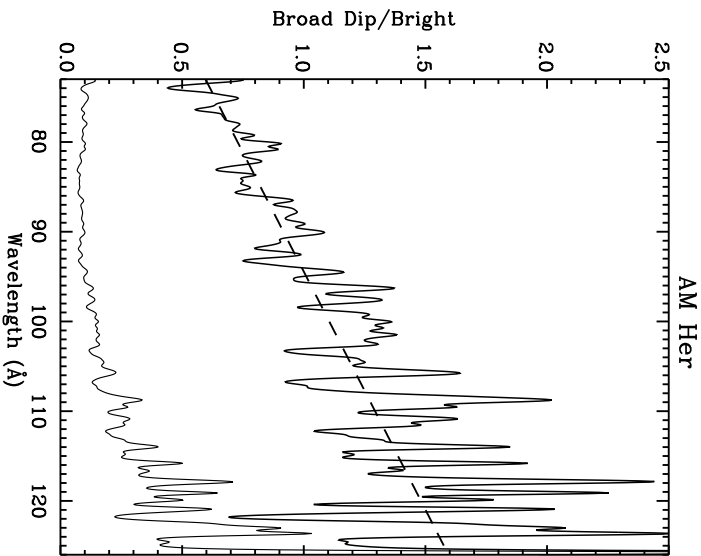
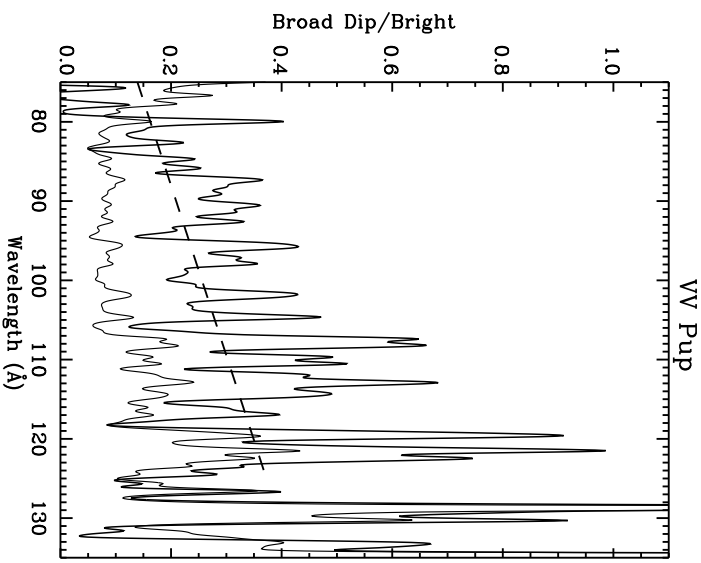
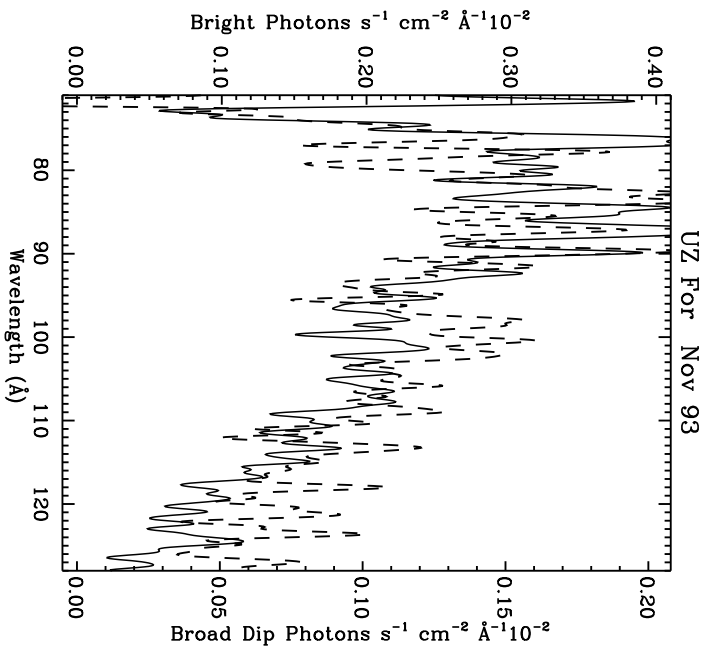
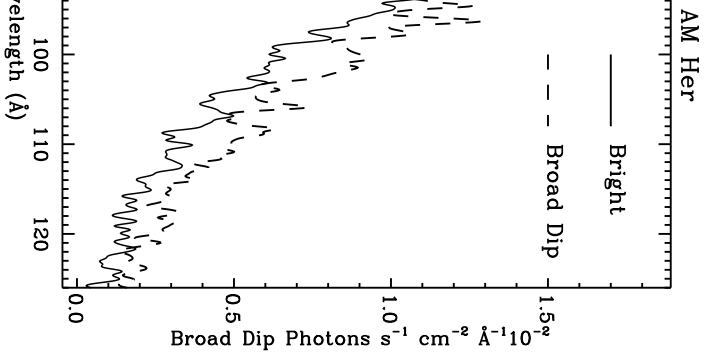
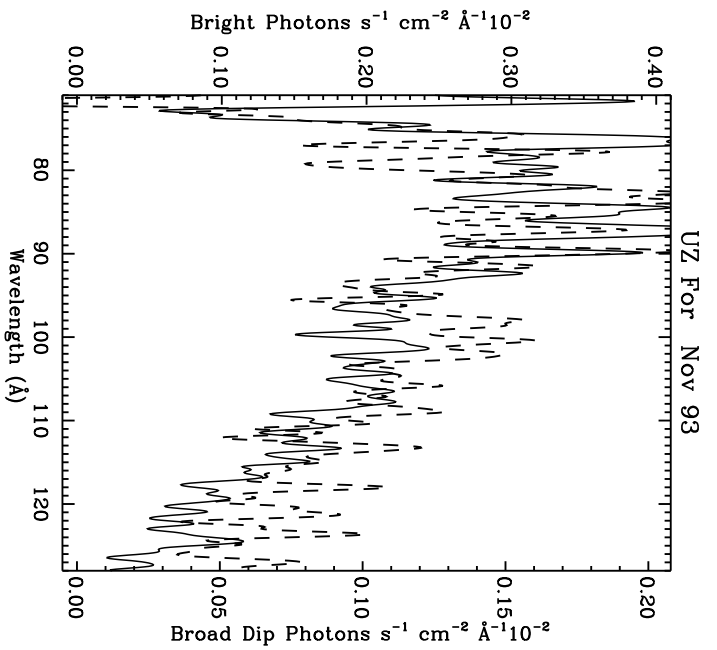
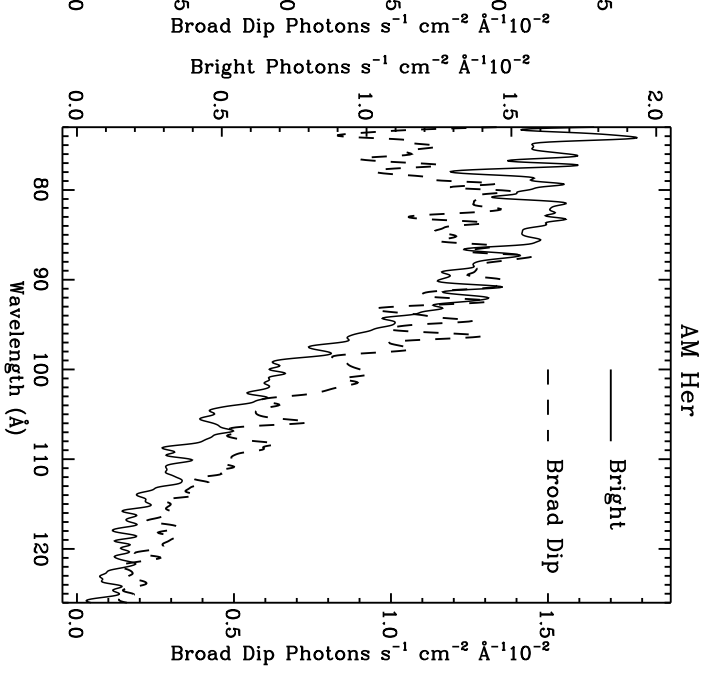
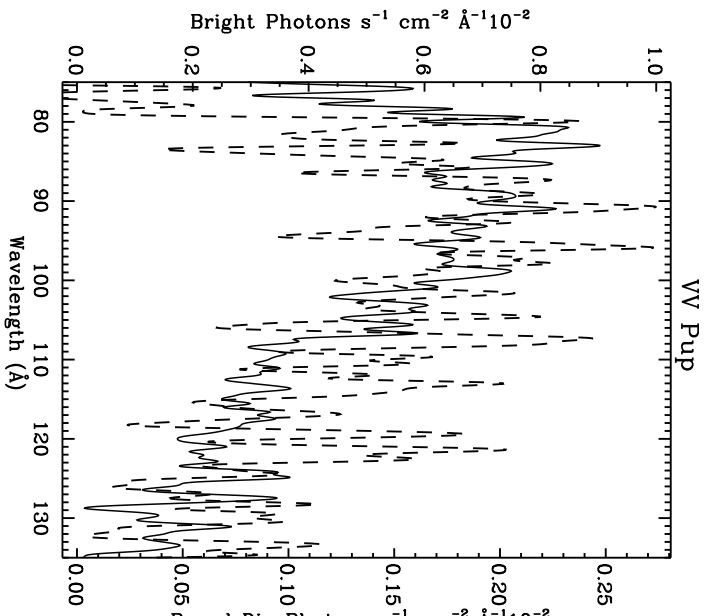




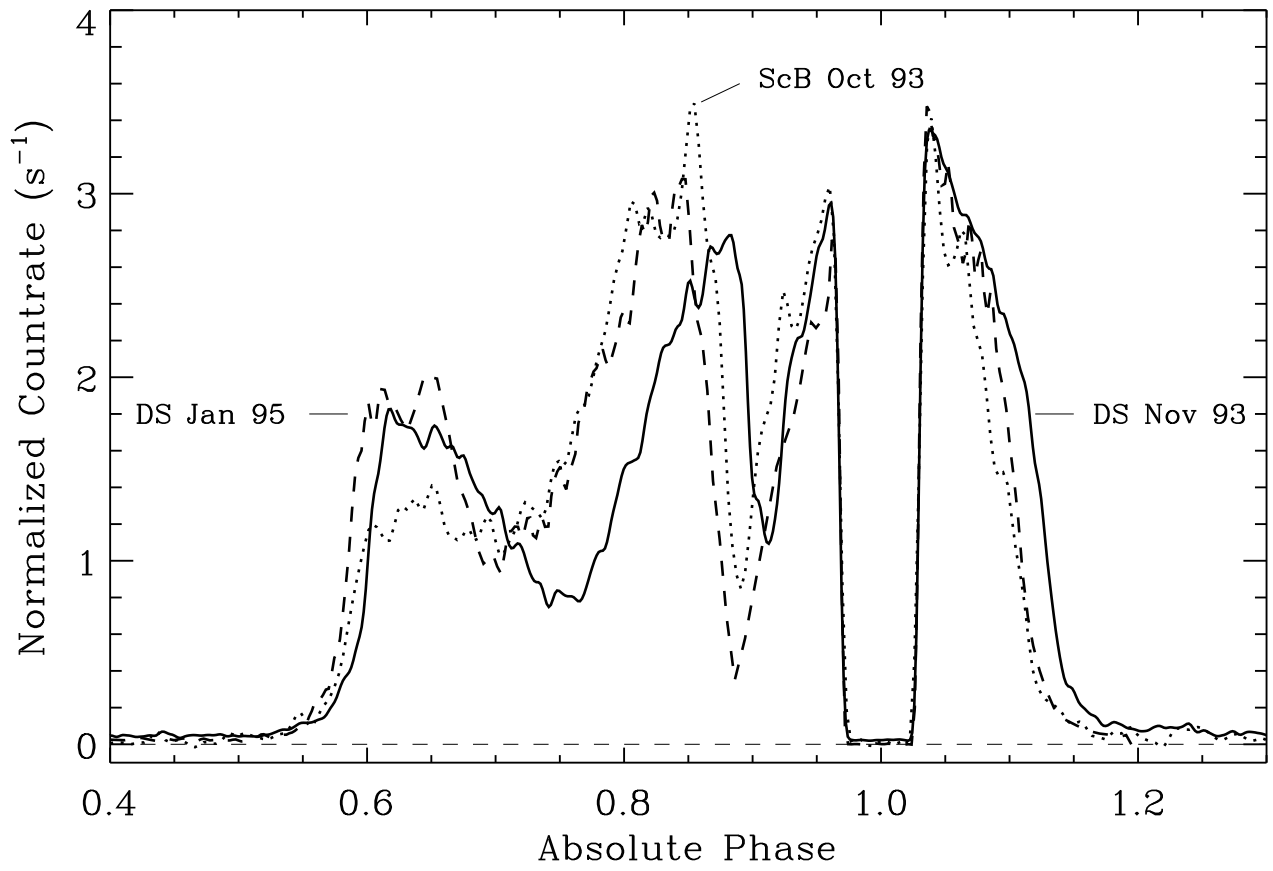








UZ For



RE1149+284

